

**FABRICATION OF POLYMER NANOFLUIDIC CHIPS
WITH PROTON BEAM WRITING AND
NANOIMPRINTING FOR DNA LINEARIZATION**

YAN PEIYAN

(B.Eng. (Hons.), NUS)

**A THESIS SUBMITTED FOR THE DEGREE OF
MASTER OF SCIENCE
DEPARTMENT OF PHYSICS
NATIONAL UNIVERSITY OF SINGAPORE
2020**

Supervisor:

Associate Professor Jeroen Anton van Kan

Examiners:

Associate Professor Wang Zhisong

Associate Professor Thomas Osipowicz

Declaration

I hereby declare that this thesis is my original work and it has been written by me in its entirety. I have duly acknowledged all the sources of information which have been used in the thesis.

This thesis has also not been submitted for any degree in any university previously.

A square image containing a handwritten signature in black ink. The signature is stylized, with a large, looped 'Y' and a long, sweeping horizontal stroke at the bottom.

Yan Peiyan

3 August 2020

Acknowledgements

Foremost, I would like to express my sincere gratitude to my supervisor A/Prof Jeroen Anton van KAN for the continuous support and guidance of my study and research in NUS. I could not have completed this thesis without his help in research methods and academic writing. Besides my supervisor, I would like to thank Dr. Shyi Herng Kan for offering the opportunities for internships and various projects.

My sincere thanks also go to professors and researchers in Centre for Ion Applications: Prof Thomas Osipowicz, A/Prof Andrew Bettiol, Dr. Ren Min Qin, Dr. Saumitra, Dr. Chan Taw Kuei, Dr. Mi Zhaohong, Dr. Liang Haidong and Dr. Jin Huining for their kindly sharing of knowledge and experience on research. I would also like to thank Prof Johan, Dr. Rajib basak and Dr. Indresh Yadav on collaboration opportunities on DNA linearization project.

Last but not least, I would like to thank Mr. Cao Yangbin, Mr. Tan Huei Ming, Dr. Tanmoy, Dr. Sarfraz Qureshi, Dr. Dou Yanxin, Dr. Gong Jintao, and Mr. Rudy Pang for teaching me on equipment operations and experimental methods. I will remember all the precious lessons I have learnt and the fun I have had in CIBA.

Contents

Declaration	i
Acknowledgements	ii
Contents	iii
Summary	v
List of tables	vi
List of figures	vii
List of abbreviation	xi
Chapter 1 Introduction	1
1.1 Overview of nanofluidic chips	1
1.2 Nanofabrication	3
1.3 Proton beam writing	6
1.4 Photoresist	9
1.5 Applications of nanofluidic devices	13
1.5.1 Nanofluidic transport	13
1.5.2 Application on DNA linearization	14
1.6 Motivation for the thesis	15
Chapter 2 Proton Beam Writing	17
2.1 Accelerator layout at CIBA	17
2.2 Proton beam writing beam line and end station	18
2.3 Proton beam writing	23
2.3.1 Sample preparation	23
2.3.2 Beam path in resist estimation	24
2.3.3 Beam focusing	25
2.3.4 Beam spot size estimation	27
2.3.5 Current measurement	32
2.3.6 Programming writing path	32
Chapter 3 Nanofluidic Chip Fabrication	37
3.1 Overview of fabrication methods	37
3.1.1 Nanopatterning methods	37
3.1.2 Lab on a chip fabrication	38

3.1.3 Pattern transfer from molds, stamps to nanoimprinted chips	41
3.2 Design and fabrication requirements.....	44
3.3 Mold making	47
3.3.1 Resist molds.....	47
3.3.2 Ormostamp fabrication.....	54
3.4 Chip replication	59
3.4.1 PMMA nanoimprinting	59
3.4.2 PDMS and X-PDMS casting	67
3.4.3 Sealing nanochannels through bonding.....	68
Chapter 4 DNA linearization and imaging	73
4.1 Nanofluidic chips application on DNA sequencing	73
4.2 DNA linearization mechanism	74
4.3 Experiment method	77
Chapter 5 Conclusions	79
Bibliography	81

Summary

Nanofluidic enclosed lab on chip (LOC) devices with nano size patterns and fast fabrication capability are required for biomedical experiments. Nanopatterning and fabrication methods for nanochannel devices are discussed with focusing on proton beam lithography, Ormostamp mold casting, nanoimprinting on PMMA and bonding procedures.

Among various nanofabrication methods and chip substrate material, several type of polymer substrates are evaluated on throughput and functionality. The most suitable method to achieve high throughput replication of the nanofluidic devices is thermal imprinting. Nanoimprinting can be completed in minutes employing a rigid stamp, proper heating and cooling systems and optimized bonding conditions. Nano ridges patterns are transferred from resist master mold to rigid stamps and polymer substrate with high fidelity and minimal distortion. This replication method is compared with PDMS and X-PDMS casting on its merits. PMMA chips are shown to be a viable candidate for DNA imaging.

These nanofluidic LOC devices are used for biomedical experiments like DNA molecules linearization and large-scale genome mapping. The cross section of the fluidic channels is chosen such that they mimic physiological condition.

List of tables

Table 2-1. Parameters set for writing a HSQ nanochannel by moving the sample stage in one direction.	33
Table 2-2. Parameters for a beam scan writing on XR1541 resist.....	35
Table 3-1. Summary of width of nanochannels on sample master mold, Ormostamp and imprinted nanochannels. The HSQ channels depth is 132 nm.....	71

List of figures

Figure 2-1 Layout of singletron accelerator in CIBA, NUS. Next generation proton beam writing facility is connected to the beamline positioned 20 degree to the upstream beamline. The picture is from [70].	18
Figure 2-2 Layout of 20 degree beam line. The quadrupole lenses are configured in spaced oxford triplet mode (CDC). Lenses 1 and 2 are coupled to the same power supply.	21
Figure 2-3 Photo of proton beam writing chamber. The beam comes from the left side. A silicon pin diode is mounted on an acrylic board which can be moved horizontally. The camera is mounted to the right side.	22
Figure 2-4 A Faraday Cup for beam current measurement is mounted with pin diode, capable of moving into and off the beam path.	22
Figure 2-5 A simulation of 750 keV protons traverse through 200 nm thick PMMA (1.19 g/cm^3) resist layer.	25
Figure 2-6 Intensity map of protons scattered from a corner of a resolution standard by scanning the beam at 2 microns range.	30
Figure 2-7 Proton counts at X direction line and fitted curve. The pixel size is 7.8 nm. FWHM of the curve is defined as spot size in X direction, which is 70.1 ± 7.8 nm.	31
Figure 2-8 Proton counts at an Y direction line and fitted curve. The pixel size is 7.8 nm. FWHM of the curve is defined as spot size in Y direction, which is 72.4 ± 7.8 nm.	31
Figure 2-9 Drawing of 50 tapered nanochannels which are written on HSQ resist by scanning 1.5 MeV hydrogen molecular beam in X and Y directions.	36
Figure 3-1 Enclosed PMMA chip using Kapton as substrate.	39
Figure 3-2 2 MeV proton writing lines connecting of a square reservoir showing end-of-range damage to bulk PMMA.	40
Figure 3-3 Optical image of 1.5 MeV molecular hydrogen ions writing on bulk PMMA forming buried channels.	40
Figure 3-4 Optical images of PMMA patterns formed by irradiating 100 keV hydrogen molecular ions over masked PMMA resist.	41
Figure 3-5 A schematic illustration of making enclosed PMMA chip by making resist master mold, Ormostamp, imprinting on PMMA and bonding method.	44

Figure 3-6 (a) Design of microchannels and reservoirs in CAD. (b) SEM image of a mr_DWL microchannel master mold.....	46
Figure 3-7 (a) Design of nanochannel array in CAD. (b)and (c) SEM image of HSQ master mold of tapered end of nanochannels.....	47
Figure 3-8 SEM images of PMMA nanochannels on silicon substrate of dimension 72×120 nm (depth \times width) written by 1.5 MeV hydrogen molecular beam with stage movement in Y direction.	50
Figure 3-9 SEM images of PMMA spincoated on Si wafer and patterned with proton beam writing. (a) Nanochannel arrays with two square markers; (b) higher magnification image. The channels are of dimension 72 nm \times 200 nm (depth \times width). The patterns are written by 1.5 MeV hydrogen molecular beam with stage movement in Y direction.	50
Figure 3-10 (a) Height profile of PMMA master mold containing nanochannel patterns from AFM. (b) Height profile histogram showing thickness of PMMA is around 72 nm.	51
Figure 3-11 High profile from AFM on HSQ microchannel and nanochannel. (a) Height profile mapping containing microsize and nanosize channels. (b) Histogram on an edge of microchannel indicating the thickness of HSQ layer is around 132 nm.	51
Figure 3-12 Optical images of nanolines formed by PBW on 132 nm thick XR-1541 resist. (a) Tapered lines were formed by sample stage movement and beam scanning in the orthogonal direction. (b) A nanolines array is formed by beam scanning.	52
Figure 3-13 SEM image of HSQ lines written by proton beam writing with dimension 132 nm \times 231 nm (height \times width). The lines are written by 1.5 MeV hydrogen molecular beam with beam scanning in X and Y directions.	52
Figure 3-14 (a) AFM characterisation of mr-DWL master mold with microchannel pattern. (b) Peak-to-peak distance showing the thickness of the DWL wall is around 5 μ m.	53
Figure 3-15 SEM image of mr-DWL microchannels with dimension 5 μ m \times 7.3 μ m (height \times width).	53
Figure 3-16 Optical images of double-layer master resist containing XR1541 nanolines and mr-DWL microlines.....	53
Figure 3-17 Schematic illustration on Ormostamp fabrication procedure. (a) Prepare a master mold; (b) prepare clean glass slide coated with adhesion promotor, apply Ormostamp on master mold; (c) UV cure Ormostamp; (d)-(f) demold	

Ormostamps from master molds and repeat the process to get an Ormostamp with the same orientation as master molds for nanoimprinting.	56
Figure 3-18 (a) AFM images of a microsize mark of PMMA master mold. (b) Peak-to-peak distance on histogram showing the thickness of PMMA is around 71 nm.	57
Figure 3-19 (a) AFM image of Ormostamp casted from PMMA nanochannel master on silicon; (b) height profile histogram showing the height of nanochannel walls around 76.5 nm.	57
Figure 3-20 AFM height profile characterization of Ormostamp, casted from the PMMA master mold as shown in figure 3-8. (a) Height profile of the Ormostamp containing nanosize ridges; (b) peak-to-peak distance in histogram showing ridges thickness around 75 nm.	58
Figure 3-21 Optical microscopy image of nanolines on Ormostamp.	58
Figure 3-22 Optical microscopy image of microlines and nanolines on Ormostamp.	58
Figure 3-23 SEM of Ormostamp casted from HSQ master resist mold with dimension 132×238 nm. (a)Nanolines connected with microlines. (b) Nanolines.	59
Figure 3-24 (a) SEM image of imprinted nanochannels imprinted using an Ormostamp which is casted from a HSQ resist mold. (b) SEM image with larger magnification. Dimension of the nanochannels is $132 \text{ nm} \times 210 \text{ nm}$	61
Figure 3-25 Imprinting chamber heating and cooling curve when imprinting is conducted, showing the chamber is held at imprinting 120°C and 20 bars for 1 minute for imprinting and cooled down.	63
Figure 3-26 Scanning probe microscopy images on three PMMA pieces imprinted with nanochannel features for (a)1, (b)5 and (c) 10 mins respectively.	64
Figure 3-27 Optical microscopy images of the three PMMA pieces imprinted with nanochannel features for (a)1,(b)5 and (c)10 mins respectively.	65
Figure 3-28 A height profile along a line scan from surface probe microscopy on PMMA imprinted for 10 mins, showing a surface roughness around 8 nm.	66
Figure 3-29 AFM images on imprinted PMMA channels, displaying percentages of height profiles (Y axis) over the height information in nm (X axis). Distances between two peaks stand for height difference on PMMA top surface and bottom surface of dented features on the pieces imprinted for (a) 1, (b) 5 and (c) 10 mins,	

showing channel depths 75.8 nm, 75.5 nm and 73.4 nm respectively. The widths of channels are not captured reliably due to tip rounding.	67
Figure 3-30 Optical microscopy images of enclosed PMMA chips, made by bonding PMMA sheets imprinted with microsize channels and nanosize channels.	70
Figure 4-1 Overview of the physical regimes in nanochannel confinements from W Reisner et.al [92]. When the channel dimensions are below the radius-of-gyration R_g , DNA molecules are characterized as isometric blobs in de Gennes regime with geometric average of the channel dimensions D , and the blobs become anisometric below a critical width D^{**} with physical extent H along the channel. At channel dimension P to $2P$, molecules are characterized as isolated hairpins with a global persistence length G . With channel dimensions below P , molecules are extended in nanochannels, characterized by the deflection length λ	77

List of abbreviation

AFM	Atomic Force Microscopy
CVD	Chemical Vapor Deposition
DI Water	Deionized water
EBL	Electron Beam Lithography
FIB	Focused Ion Beam
HSQ	Hydrogen silsesquixane
IL	Interferometric Lithography
IPA	Isopropyl Alcohol
MEMS	Micro-electromechanical System
NIL	Nanoimprinting Lithography
PBW	Proton Beam Writing
PC	Polycarbonate
PDMS	Polydimethylsiloxane
PMMA	Poly-methyl methacrylate
PVD	Physical Vapor Deposition
RIE	Reactive Ion Etching
SEM	Secondary Electron Microscopy
SL	Sphere Lithography
SPM	Scanning Probe Microscopy
SRIM	Stopping Range of Ions in Matter
TMAH	Tetramethylammonium hydroxide
UV	Ultraviolet

Chapter 1 Introduction

1.1 Overview of nanofluidic chips

The applications of microfluidic and nanofluidic chips make use of the physical parameters change as the system shrink down to micron or nano size. In the expression of the Reynolds number, $Re = \rho v D_h / \mu$ where ρ , v , D_h and μ stands for fluid density, characteristic fluid speed, channel diameter and fluid viscosity, small channel diameter D_h makes the Reynolds number small [1]. In micro channels, Reynold number is around 10^{-3} . Different with meso and macroscales phenomenon, fluid experiences laminar flow where viscous force dominates, and the behaviors of particles in the fluid can be predicted [2]. At micron size, fluid behaves like massless particle because inertial force decreases faster than viscous force when devices scale down. Mixing two streams happens at the interface area by diffusive effect. For the application of separating particles with different sizes, the particles diffuse from high to low concentration and diffuse at different speeds corresponding to the sizes. Separation of proteins and smaller DNA molecules which contain less than a thousand base pairs is achieved using arrays of nanopillars to clog with large molecules [3] and introducing molecules to arrays of wide and narrow channels. Smaller molecules enter narrow channels and travel a longer path while large molecules move smoothly through wide channels but excluded from narrow channels [4]. There is capillary effect in micro and nano size channels. Electro kinetic actuation is more efficient in driving fluid flow to certain flow rates

and are therefore more widely used in fluidic chip applications. In electrophoresis, fluid flows uniformly in direction of electric field because of convection of liquid flow created by the electric double layer [5][6].

Nanofluidic lab on chip devices are widely used in biological applications, saving on usage of expensive and small volume reagents and samples [7]. Combined with lab-on-a-chip devices, experiments on molecules can be conducted with small volumes and simplified setups with high resolution. Nanofluidic lab on chip devices are used in single molecule detection including DNA fragment sizing, detection of quantum dots with fluorophores and fluorescence labeled proteins [8]. It provides a cheaper and faster way of DNA sequencing by shearing, confining and linearizing the segments. Faster processing can be achieved by massive parallelism and advanced bioinformatics tools. Moreover, micro/nano fluidic lab on chip devices made portable analytical tool possible by integrating the channel structures with different laboratory functions [9][10]. Micro and nano-size channels make application of higher-concentration single molecule detection possible by constraining the observation in an environment much smaller than the laser focal volume. It increases signal-to-noise ratio as out-of-focus background fluorescence is reduced. Integrated with laser and detection setup, detection can be implemented in parallel detection volume with improved efficiency. Nanofluidic LOC devices also play an essential role in investigating single polymer and intramolecular dynamics of double stranded DNA as the nano space confinement induces slowing down of intramolecular fluctuation, which enables DNA motion control and sequence readout [11]. Polymers like PDMS and PMMA have been developed as

material for high throughput fabrication with desired properties like optical transparency, lower auto-fluorescent background compared with other polymers and relative low price.

1.2 Nanofabrication

Nanofabrication of nanofluidic devices have been developed for different aspect ratio structures requirements including 0-D nanopores, 1-D nanotubes and 2-D nanoslits [12]. Lithography methods are applied to form nanosize patterns through photochemical reactions when light or ion beam strikes the resist and induces polymer chain break-up or crosslinking [13], such as electron beam writing (EBL) [14], focused ion beam writing (FIB) [15] and UV lithography. In photolithography, pattern resolution is restricted by diffraction limit which is typically about $\frac{1}{2}$ to $\frac{1}{4}$ of the wavelength of light involved [16]. In the case of UV lithography, the resolution limit is about 100 nm [17]. Wavelengths of energetic ion beams relates to the given energy of the beam, as shown in the de Broglie relation $\lambda = \frac{h}{p}$ where λ , h and p stand for the de Broglie wavelength, Planck constant and the momentum.

Applied with 1kV accelerating voltage, electron beams have wavelengths $\lambda_e = \frac{h}{p} =$

$$\frac{h}{\sqrt{2em_eU}} = \frac{6.63 \times 10^{-34} J \cdot s}{\sqrt{2 \times 9.1 \times 10^{-31} \times 10^3 \times 1.6 \times 10^{-19}}} = 3.89 \times 10^{-11} m.$$

A proton beam which has 1 keV energy has wavelength $9.05 \times 10^{-13} m$. The wavelengths of energetic ion beams are much smaller than 1nm, thus they are capable of imaging and patterning with nanometer resolution. Electron beam writing is applied to pattern resist in a direct writing mode followed by substrate (silicon and silicon dioxide) etching

[18][19]. Focused ion beam technique is utilized to make nanoscale trench directly on hard substrates by introducing energetic gallium ions to target surfaces, providing enough energy for target atoms to escape from the surface through a cascade of collisions [15][20]. FIB has been applied to fabricate nanopores through thin membranes [21] and nanochannels parallel to the surface[22][23]. However, the methods are time-consuming and not suitable for large scale structure writing. Nanoimprinting lithography (NIL) [24][25], interferometric lithography (IL) [26] and sphere lithography (SL) [27] are methods for large scale nanopatterning. Patterns can be transferred to silicon-based material by MEMS based approaches, which contains standard photography followed by additive deposition or subtractive etching process. In sacrificial layer releasing method, male form of nanochannel pattern is formed on the sacrificial layer followed by deposition of capping layer, making access reservoirs and releasing nanochannel [28]. Bulk etching can be done by reactive ion etching for silicon substrate (RIE), chemical etching [29] and thin film etching. Various materials are available for etching and deposition methods. However, there are drawbacks on long etching time and dependency on costly equipment and low fabrication yield. Channels are bonded to another substrate to enclose the chip. In anodic bonding method, chemical bonds are formed between silicon and glass when high DC voltage and 400 °C conditions are applied[30]. Thermal fusion bonding is applied to two materials having similar thermal expansion coefficients, heating to a high temperature near to glass transition temperature. Polymer chips and films are bonded by the strong diffusion and plastic deformation at the interface [31]. An adhesive layer can be used during

bonding and clean and defect-free surfaces are also required to successfully bond substrates [32][33]. Non-conformal deposition can be used to make self-sealing nanochannels using CVD and PVD [34][35]. However, final channel width is hard to control. Edge lithography makes use of standard lithography patterning thin metal layer and makes metal mask by selective metal etching. Nano trenches are formed by deep reactive ion etching (DRIE) with the mask [36].

There are nanofabrication methods based on nanomaterial which has morphological feature size at nanoscale. Ion selective polymer made by contact lithography attracts counter ions and repel co-ions from entering nanopores [37]. Nanowire and nanotubes can be applied as template or sacrificial layers for nanochannel fabrication while alignment is challenging, and throughput is low. Nanoporous membrane and nanoparticle crystal with surface functional groups are applied in photonic and biological sensors, exhibiting advantages in low cost, simple and fast fabrication and large effective area. However, size-controllability and batch-to-batch repeatability is low, which is hard to be applied to large throughput nanochannel fabrications [38][39]. Various factors should be considered in fabrication including the size and material requirements for specific applications, nanopatterning ability, size controllability and compatibility with other techniques. The cost in material, facility and operation is to be considered.

Fabrication of nanofluidic chip for DNA linearization that is discussed in this thesis is achieved combining proton beam writing, stamp fabrication, NIL and bonding if required. Nano patterns are written on photoresist and transferred to stamps and chip materials. Besides direct writing or UV lithography, nanoimprint lithography

provides a way to transfer patterns to polymer with high throughput. A stamp is pressed into a polymer at temperatures above the polymers' glass transition point pressed into cavities of the molds as polymer reflows. The polymer is cooled down and solidified to hard-glassy state. Then the pressure inside bonding chamber can be released and demould the imprinted polymer. Resolution of patterns on chips depends on writing resolutions, capability of stamp material to form straight side walls, durability of stamps and properties of chip materials like PMMA and PDMS. Patterns can also be transferred to different materials for various applications. Diamond and nickel stamps exhibit high durability and features around one hundred nanometers in imprinting processes [40][41][42][43].

1.3 Proton beam writing

Proton beam writing is used in the fabrication of microfluidic chips by producing structures on photoresists through the stage and sample movement or beam scanning in horizontal or vertical directions. With massless, three-dimensional process and direct write capability, proton beam writing plays a leading role in next generation lithography with the capability of high aspect ratio structures and potentials in various applications including material modification on Si and diamond, sensors, lab-on-a-chip technology and rapid prototyping of optical circuits [44][45][46].

Compared to optical lithography, which is constrained by diffraction limit, direct writing methods provide better solutions to better resolution circuits manufacturing. The de Broglie wavelength of 1 keV electron is around 0.04 nm while the

wavelength of UV is 10 to 400 nm. In electron beam lithography, high energetic electrons broaden the trajectory and the proximity effect results in the broadening of final written structures. The large nuclear to electron mass ratio results in minimal proximity effect in written structures caused by an energetic proton beam. At the same time the even energy deposition of the proton beam results in straight and smooth side walls as well as high aspect ratios [47][48][49]. Thus, high-aspect-ratio nanochannels can directly be formed on resist without selective etching, opening up possibilities which are not available in other techniques [50]. High penetration of proton beam makes PBW feasible in patterning thick photoresist, Si patterning and buried channel patterning in Polymethyl Methacrylate (PMMA). Buried channel patterning at the end of range of the proton beam is based on the mechanism that the protons energy loss is order of magnitude higher at the end of the range than the surface region [51]. In this thesis, proton beam writing is used in patterning photoresist PMMA, AZ1518 and HSQ in order to get high aspect ratio ridges or grooves with minimal side wall broadening.

Proton beam writing is implemented using a 3.5 MV high brightness High Voltage Engineering Europa Singletron™ ion accelerator [52]. With object apertures, collimator apertures and four magnetic quadrupole lenses, beam is reported to be focused down to $19.0 \times 29.0 \text{ nm}^2$ [52]. In the end station, a pin diode is mounted behind the sample stage to detect forward scattered beam and an electron detector is mounted in front of stage to collect secondary electrons. The beam is scanned by electrostatic scanning system, which is aligned and capable of scanning the beam at $100 \times 100 \text{ }\mu\text{m}^2$. The beam writing is assisted by movement of precisely

controlled PI N-310K059 stage with 4 nm closed loop and 20 mm movement range in both directions. The stage can move in Z direction in 20 mm range to place the sample surface in pre-defined focal plan of the beam. By scanning the beam on a 1 μm thick nickel grid, which contains 5 μm wide grid bars 25 μm spaced apart, forward scattered beam and transmitted beam is collected by positive biased pin diode and secondary electrons generated from the metal grid is collected by the electron detector. Beam collected by both detectors is amplified and mapped in single channel analyzer forming a 2D map of scattered ions or electrons. By moving the stage and comparing the grid images before and after stage movement, beam scanning size is calibrated and the pixel size in grid image is calculated. Beam counts along lines in X and Y directions are extracted and fitted using the error function. Full-width half-maximum of fitted line scan profiles provides the beam spot size in X and Y directions. By controlling the exposure time and stage movement speed, photoresist is exposed to proton beam with certain dose, varied according to types of photoresist, thickness of samples, width of structures and writing areas.

Photoresist is developed and post-baked, if required, after proton beam writing. The exposed area shows chain-scission for positive resist and is cross-linked for negative resist. Photoresist is chosen according to required pattern, thickness, hardness and sensitivity. In the experiments conducted in this project, photoresist is spin-coated on Si wafer and patterned by proton beam or laser. The pattern is transferred to Ormstamp and imprint on PMMA to form nanofluidic chips for various applications.

1.4 Photoresist

Photoresist is used in proton beam writing to form primary structures on a substrate. Using proton beam writing, protons with MeV energy penetrate photoresist in straight path. Protons mainly interact with resist electrons and induced secondary electrons modify the molecular structures, which causes polymer chains crosslinking or scission [53]. Being dissolved in solvent, photoresist can be spin coated on a substrate. Thickness can be controlled through different spin coating speeds while calibration work is necessary in fabrication when structure dimension is critical. Thickness of coated resist varies with polymer types, solvent content and surface properties of substrate. Pre-bake evaporates excessive solvent. PMMA (formerly Microchem Corp.), SU-8 (formerly Microchem Corp.) and HSQ (Dow Corning) are used in micro and nanofabrication for their high resolution. After radiation, post-bake and developing, structures can be transferred to PMMA sheets (PLEXIGLAS®) through imprinting or Polydimethylsiloxane (PDMS, SYLGARD 184™, Dow Corning) through casting for microfluidics applications. Being exposed to light or ions, long chains in positive resist polymer are cut by photoelectric electrons or secondary electrons and the resist become soluble in corresponding developers. For negative photoresist, chains are cross-linked after photon or ion irradiations and the exposed area become insoluble in developers. Dose required for clear cross-link or chain-scissoring photoresists varies with type of developers, developing time and methods, thickness of resist, type and energy of ions or molecules. Dose should be well-controlled to achieve chain-scission or polymer crosslinking. Exposing positive resist with large dose may cause cross-

linking and the exposed polymer is insoluble to developers. Post-exposure delay may cause variations in properties like sensitivity and contrast for some resist. In this project, PMMA, HSQ and SU-8, whose sensitivity and contrast are less effected by processing conditions other than ion dose and resist thickness, are used for forming patterns for fluidic chips.

Contrast of photoresist relates to the developing rate as a function of exposure dose [54]. Higher contrast indicates a possibility of fabricating structures with higher aspect ratio and vertical sidewalls. Sensitivity of positive resist is defined as the smallest dose needed for completely removing the resist. It is represented by the contrast curve as a function of logarithmic exposure dose with respect to removed or cross-linked photoresist thickness [54]. For negative resist, sensitivity describes the smallest dose needed for making half of the original thickness of the resist insoluble in developers.

PMMA

Polymethyl Methacrylate ($(C_5O_2H_8)_n$) (PMMA) is a positive photoresist used in Ni mold fabrication because of high resolution, wide range of thickness achievable compared to HSQ and feasibility in removing compared to SU-8. Properties including non-toxic nature of solvent, non-sensitivity to white light, long shelf life and no processing delay effects make it an ideal candidate of resists for lithography. PMMA is reported to be able to achieve features written by proton beam with 20 – 30 nm dimension. A minimum energy of 3.4 eV can achieve chain scissoring. [53] Dose needed is 80 – 150 nC/mm², depending on developer type[55]. PMMA is

suitable in Ni mold fabrication as it is capable of forming high resolution structures with focused proton beam and it is easy to remove. Parallel lines with width 50 nm in 350 nm-thick PMMA is reported in making Ni molds using nickel sulfamate electroplating[55]. Direct beam writing can be done in spin coated PMMA resist with thickness 100 nm to tens of microns and in PMMA sheet (PLEXIGLAS®) which can be hundreds of microns thick. Buried channel waveguides in PMMA have been fabricated by using 1.5 MeV and 2.0 MeV proton with dose 1.6×10^{13} to 1.0×10^{14} ions/cm²[45]. 50 nm narrow walls with aspect ratio 7 is produced with PMMA[56].

Isopropyl alcohol with deionized water in ratio 7:3 is capable of dissolving the patterns written in smaller dose. Compared to GG developer, which is a mixture of 15 vol.% water, 60 vol.% 2-(2-butoxyethoxy)ethanol, 20 vol.% tetrahydro-1,4-oxazine (morpholine) and 5 vol.% 2-aminoethanol [53], the 7:3 IPA:DI water developer requires 10 times shorter time for developing nanostructures due to smaller viscosity.

GG developer shows better sensitivity (7.5×10^{13} ions/cm²) compared with 7:3 IPA/DI water developer (9.5×10^{13} ions/cm²) in developing 2.4 μ m thick PMMA resist which is patterned by 2 MeV proton beam as reported in [57]. Using developer methyl isobutyl ketone (MIBK)/IPA 1:3 solution requires larger dose (2.5×10^{14} to 3×10^{14} ions/cm²) to dissolve exposed polymer throughout [58]. Contrast value of resist developed by GG developer is larger than the one developed by IPA/DI water. It is also observed that developing in ultrasonic agitation reduces the developing time. In this project, developing is done by using GG developer at

30 °C to develop micro size structures following by dipping substrates into 7:3 IPA/DI water solution to develop nano-size lines structures.

HSQ

Hydrogen silsesquioxane (HSQ) is a negative photoresist. 4.08 eV and 8.95 eV are needed to break Si-H and Si-O bonds in hydrogen silsesquioxane and form crosslinked network [53]. It achieves 19 nm line width with 100 nm thickness by 2 MeV proton beam writing. The sensitivity is 1.9×10^{13} - 1.3×10^{14} ions/cm² and contrast is 1.2 to 10, depending on the HSQ batch. HSQ is developed in 2.38% tetramethyl ammonium hydroxide (TMAH) solution for 1-2 minutes followed by a DI water rinse. Capability of forming high resolution patterns makes HSQ a viable candidate in nanofluidic chips fabrication. The drawback of HSQ is relative short shelf-life and variations of sensitivity and contrasts which is highly depend on processing conditions as well as batch. In fabrication process, no primer is required before spin coating HSQ onto Si substrate. Ti thin layer (2-4 nm) can be sputtered on Si substrate to enhance adhesion before spin coating thick HSQ resist layer [59]. It is reported that delay between soft bake and beam exposure for 1 week in air decreases the sensitivity and enhances the contrast. Delay in both beam exposure and developing should be avoided in order to get patterns in good resolution [60].

SU-8

SU-8 is a negative tone photoresist, capable for high resolution high aspect ratio structures. 16 nm wide line with 10 μm thick SU-8 structure is fabricated using 1 MeV protons in CIBA with 1.9×10^{14} ions/cm² dose [53]. Post exposure bake at

100 °C for 2 mins improves on rigidity of SU-8 structures, which increases the mold life in PDMS casting. Difficulty in removing cross-linked SU-8 limits its application in Ni mold fabrications.

1.5 Applications of nanofluidic devices

Nanofluidic devices have been applied in biological fields experiments such as single molecule analysis, platforms for biosensing and sample preconcentration and separation. Nanopatterned devices are also solutions for energy conversion and storage, and water purification [31].

As a direct writing lithography method, proton beam writing provides features with smooth straight side walls with high aspect ratio because of large penetration range. Multilevel structures can be written by varying the energy of the ions.

1.5.1 Nanofluidic transport

Molecules transport in nanofluidic chips is often assisted by electric field applied across the channels. Electro kinetic transport is based on the electrophoretic mobility of the molecules and electroosmotic flow. Different chip material results in the difference in surface charge of channels and difference in electroosmotic flows. Electrical double layer (EDL), consisting of stern layer and diffuse layer, shielding the surface charges from the external electrical potential [5]. The stern layer is made of immobile ions, which carries opposite charges compared to the channel wall. The mobile diffuse layer is outside of the stern layer, separated by a shear plane with the electric potential named zeta potential ζ . EDL can be explained

by the Poisson-Boltzmann equation: $\nabla^2\psi = \frac{d^2\psi}{dz^2} = \kappa^2\psi(z)$, in which z is channel surface normal direction and κ is the Debye-Hückel parameter. $\kappa = \lambda_D^{-1}$ where λ_D is Debye length describing the length where the potential dropped to e^{-1} of the original potential [6]. For ionic strength from 10^{-2} M to 10^{-4} M room temperature conditions, the Debye length can be estimated to be 3 ~ 30 nm. In microchannels, the Debye length is negligible while in nanochannels, EDL occupies a significant space. Molecular separation in nanochannels can make use of the ionic concentration gradient induced by the equilibrium between electromigration and diffusion of ions in nanochannel electrophoresis [61]. Hydrostatic pressure driven flow depends on the external driving pressure and the cross-sectional area of the nanofluidic channel. Operating pressure is limited to bonding strength between cover plate and chip substrate and Young's modulus to prevent deformation.

1.5.2 Application on DNA linearization

Nanofluidic chips fabricated using direct writing on PMMA and SU-8, Ni electroplating, Ormstamp imprinting and X-PDMS casting is used in stretching and linearizing DNA molecules for genetic profiling [62]. Nanochannels trap molecules without chemical modification thus enabling observations on conformational responses of single molecules [63] and in situ control of environmental conditions like ionic strength of buffer solution [64].

DNA segments are hard to be resolved under fluorescence microscopy when it is at a bulk phase. Single DNA molecules are stretched by confinement inside a nanochannel with tens to hundreds of nanometer cross section diameter [65]. When

the persistence length of DNA is smaller than the diameter of a nanochannel, DNA forms blobs. DNA molecules are introduced to nanochannels by pressure or electric force and stretched close to its contour length. Information on the protein-nucleic acid interaction at the level of single molecules is obtained with technologies including site-specific labeling by nicking or restriction endonucleases. DNA stretching inside nano fluidic chips achieves high throughput with arrays of parallel channels and integrated lab-on-chip devices. In nanochannels with cross section with 100 nm diameter, gene information can be obtained by probing unpaired bases on single-stranded DNA. Compared to genetic profiling of double-stranded DNA molecules, self-annealing of unpaired bases and molecules aggregation are prevented. Bases are stained using site-specific dyes and thus, genetic profiling is mapped with fluorescence imaging [62]. LOC devices with a nanochannel network enables observations of DNA metabolism such as conformational response to environmental solution conditions [64], gene expression and sequence readout because nanospace confines, stretches molecules and slows down the intramolecular thermal fluctuation [11].

1.6 Motivation for the thesis

Nano-size confinements provide possibility of observation on single molecule properties. Polymer chips have advantages of low cost, fast production and high detection throughput with parallel channels. PDMS and PMMA are bio-compatible and can be one-time-use bio chip material. Rigid nano-patterned stamps combined with nanoimprinting methods meets large quantity chips replication requirements for providing a fresh chip for every experiment.

Analysis on single-strand DNA is especially interesting for the possibility of getting physical insights from single DNA molecule from a cell, which is extracted from the mean value from a large population of DNA molecules and cells in traditional analysis methods [66]. Linearization and analysis on single strand DNA molecules have been achieved with sub-100nm cross section nanochannel devices and the stretch to a length comparable to double-strand parent DNA has been observed with biopolymer coatings on DNA molecules. To image HER-2 segments in DNA molecules for breast cancer diagnosis, nanochannel longer than 150 μm is required for imaging whole molecule and higher imaging throughput. Nanochannels are designed with tapered end for easiness in introducing molecules in.

Chapter 2 Proton Beam Writing

2.1 Accelerator layout at CIBA

Proton beam writing is conducted at Center for Ion Beam Application with the High Voltage Engineering Europa 3.5 MV Singletron [67]. The RF driver supplies energy to an oscillator circuit containing a coil and cylindrical dynodes, as shown in figure 2-1 (1), and ions are extracted by electric fields (2). The facility is capable of providing singly charged protons, hydrogen molecule ions, deuterium or alpha particles for experiments including proton induced X-ray emission (PIXE), Rutherford backscattering spectrometry (RBS), scanning transmission ion microscopy (STIM) for applications on micro machining, advanced material research and nuclear microscopy of biomedical samples [68]. The 90° double focusing magnet (4) and the slit feedback system (5) stabilize terminal voltage, minimizing the influence from temperature fluctuations to terminal voltage stability as the capacity of SF₆ gas changes with temperature. Terminal voltage ripples are minimized by a filter and a feedback circuitry, in which way the HVEE accelerator generates beam with measured stability ± 20 eV ($\sim 10^{-5}$) under laboratory conditions and terminal voltage ripple 25 V_{pp} ($\sim 1.1 \times 10^{-5}$) [69]. Thus, focused proton beam can be directed to samples for writing purposes with calibrated dosages and minimal chromatic aberrations, which is a critical requirement for superior beam focusing.

Beam is directed by steerers (3), 90 ° magnet (4) , object apertures (in between (5) and (6)) (Oxford Microbeams OM10), switching magnet (7) collimator apertures

(8) attached with micrometers, electrostatic scanning system (9) enabling beam scanning in X and Y directions and four magnetic quadrupoles lenses (10) along the proton beam line. The beam can be deflected away from the beam line by a blanking plate (6). Combining with the electrostatic scanning and the sample stage movement, patterns can be written with proton beam.

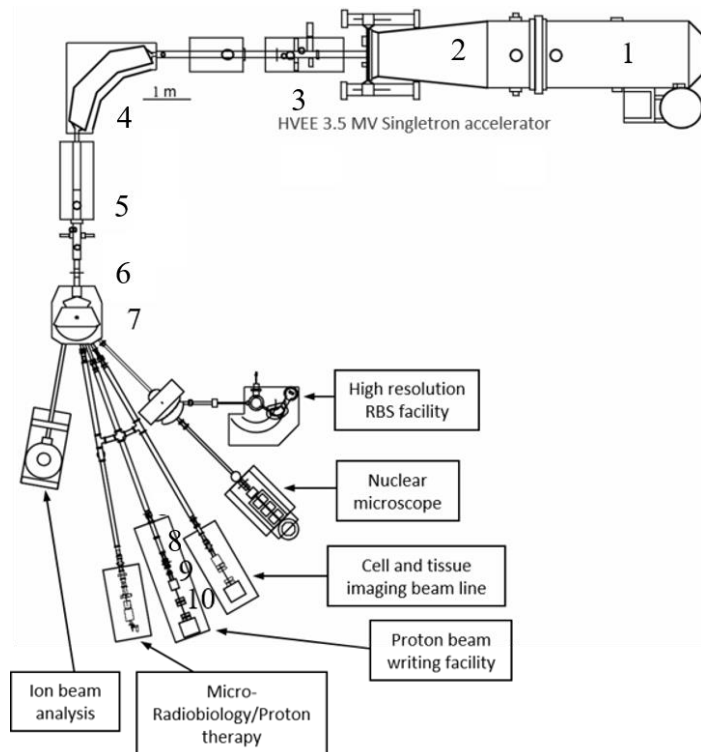


Figure 2-1 Layout of singletron accelerator in CIBA, NUS. Next generation proton beam writing facility is connected to the beamline positioned 20 degree to the upstream beamline. The picture is from [70].

2.2 Proton beam writing beam line and end station

Chamber for proton beam writing is located at the end of 20 degree beam line (Proton beam writing facility, see figure 2-1), placed on an optical table to minimize vibrations. It is equipped with high excitation triplet of compact quadrupole lenses (OM52-Oxford Microbeams) spaced in converging-diverging-converging

configuration [71]. The lenses are powered by Bruker power supplies with 1 ppm/°C and 5 ppm stability and maximum current allowed is 120 A [72][73]. Compact lens system results in higher demagnifications (857 in X direction and 130 in Y direction) but higher spherical aberrations [67].

Collimators can be adjusted with 1 μm accuracy. Two deflectors are driven by electrostatic amplifiers (7224 AE Techron, 75 μV noise level), placed before the quadrupole lens systems to scan the beam in X and Y directions in the range of around 100 μm [72]. The system demagnification is 857×130 in X and Y respectively. Different voltages are required in X and Y to get uniform scan fields. Beam writing is performed by moving of PI N-310K059 XYZ translation stage with 4 nm closed loop control for X and Y direction motions and open loop for Y direction movement. The stage is able to move in X, Y and Z directions in 20 mm range [72]. Ion beam can be focused down to 50 nm by scanning over a metal mesh grid as resolution standard manufactured by proton beam micromachining while tuning quadrupole lenses. It has advantages as resolution standard for focusing micro beam because of straight wall structures and smooth surface compared to commercially available gold mesh grid and e-beam test chip [74]. A Ni grid with 5 μm wide grid bars spaced 25 μm apart is mounted on the sample stage for beam fine focusing, scan size calibration and beam spot size estimation. It is fabricated with orthogonal ($90.0^\circ \pm 0.1^\circ$) with side wall projection smaller than 6 nm [75]. To collect both the beam passing through the Ni grid spacing and the beam penetrating through 1 μm Ni, a passivated implanted planar silicon detector (Hamamatsu, S1223) is mounted behind the sample stage for ions detection.

Ion induced secondary electron detection is used as an alternative to on- and off-axis scanning transmission ion microscopy for beam size characterization. When ion beam scans over the resolution standard, ions interact with grid bar electrons and the electrons are excited or ejected from their orbit. Micro-channel plate (MCP) is mounted around beam line inside the chamber to collect secondary electrons. It has higher detection sensitivity compared with off-axis STIM, longer life-time as a detector and enhanced imaging quality compared to pin diodes [75]. Large current and longtime measurement does not deteriorate the sensitivity of MCP; thus it is an alternative for mapping ions scanning on grid bars for longer time. MCP used in the experiments are of model NVT2C45/C4M10, mounted 8 mm away from sample stage. 2800 V back plate voltage and 100-150 V bias leads to optimum gain and collection efficiency [76]. 92 ± 5 % electron collection efficiency is reported with 500 keV hydrogen molecular ions on fabricated Au resolution standard [77]. Data acquisition system supports fastest imaging speed at 1MHz pixel update frequency. During writing, pixel update frequency is less than 100 kHz to avoid image distortions due to the relative slow slew rate of Techtron electrostatic amplifiers.

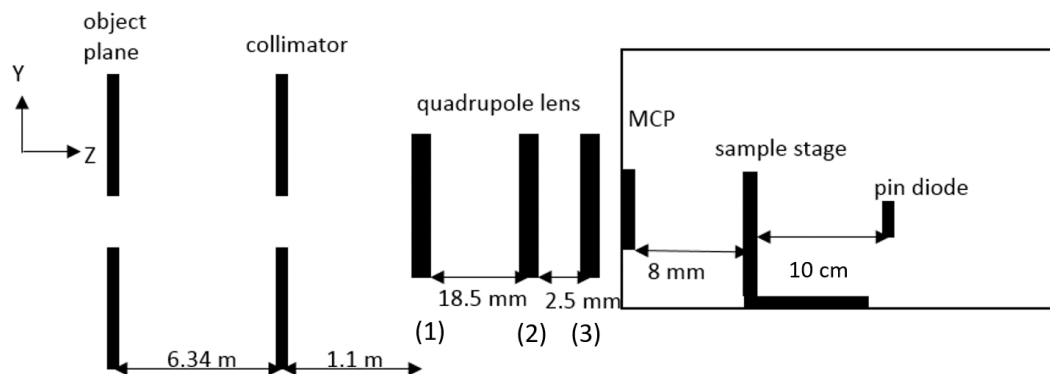


Figure 2-2 Layout of 20 degree beam line. The quadrupole lenses are configured in spaced oxford triplet mode (CDC). Lenses 1 and 2 are coupled to the same power supply.

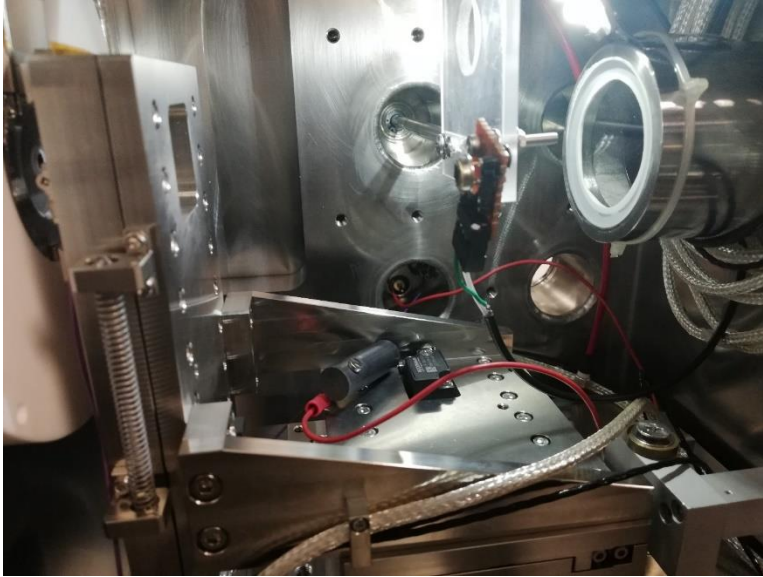


Figure 2-3 Photo of proton beam writing chamber. The beam comes from the left side. A silicon pin diode is mounted on an acrylic board which can be moved horizontally. The camera is mounted to the right side.

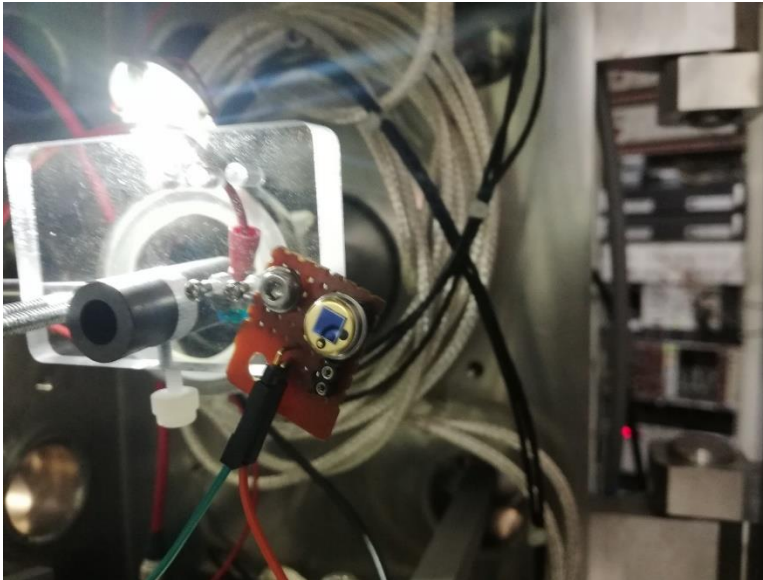


Figure 2-4 A Faraday Cup for beam current measurement is mounted with pin diode, capable of moving into and off the beam path.

2.3 Proton beam writing

2.3.1 Sample preparation

A Si substrate is coated with 20 nm thick Cr as adhesion layer and 60 nm thick Au as seed layer for Ni electroplating using magnetron sputter machine. Thinner seed layers can be coated for a better surface smoothness. Si substrate is baked at 200 °C for 5 mins to evaporate water on the surface before coating photoresist. PMMA A2 is used at spin speed 500 rpm for 10 seconds followed by 1000 rpm for 45 seconds to coat 100 nm thick layer on substrates. Pre-bake at 150 °C for 5 mins removes the excess solvent in spin-coated resist. Substrate is cut into pieces with dimensions around 20 mm by 10 mm to fit on the 20-degree beam line stage.

The height difference between substrate surface after mounting on the sample stage and the center of Ni grid bars is measured using an optical microscope. This done to guarantee the sample can be positioned in the focal plane during PBW experiments. The distances between sample and the center of grid bars in X and Y directions are measured, for the ease of finding correct writing stage positions during beam writing. The stage which is mounted with substrate is slotted into the beam line end station chamber. Rough pump can bring the vacuum level of chamber to 1.6×10^{-2} mbar, followed by pumping using turbo molecular pump and a roughing pump system, which is able to bring the vacuum level below 2.0×10^{-6} mbar for around 1 hour.

2.3.2 Beam path in resist estimation

Projected range of ions is calculated in SRIM before conducting experiments. 2 MeV protons projects 65.31 μm in PMMA (density 1.19 g/cm^3). The projected range for 1.5 MeV molecular hydrogen ions can be estimated with the simulation results of 750 keV protons, which is 12.64 μm to 15.53 μm . Secondary electrons induced by protons have relatively low energies and therefore the electron cascades are within limited range away from a proton track.

Doses needed to fully bond-scission the polymer relates to linear energy transfer of ions to the material or so-called stopping power. Energy transfer from elastic collision of ions and substrate nucleus is around three orders smaller than the energy transfer from inelastic collision of ions and substrate electrons at the end of range.

A simulation on transmitted 750 keV protons into 1.19 g/cm^3 PMMA resist is done in SRIM. The lateral straggling range is calculated from the lateral position Y and Z: $R = \sqrt{(\text{lateral } Y)^2 + (\text{lateral } Z)^2}$. 90% of the transmitted ions after traversing 200 nm are within a lateral range of 0.6 nm, which is much smaller than the nanochannel dimension requirement. Thus, proton beam penetrates into polymer resist layers in a straight path with lateral straggling smaller than 10nm. It is suitable for pattern nanochannels which have width smaller than 100 nm.

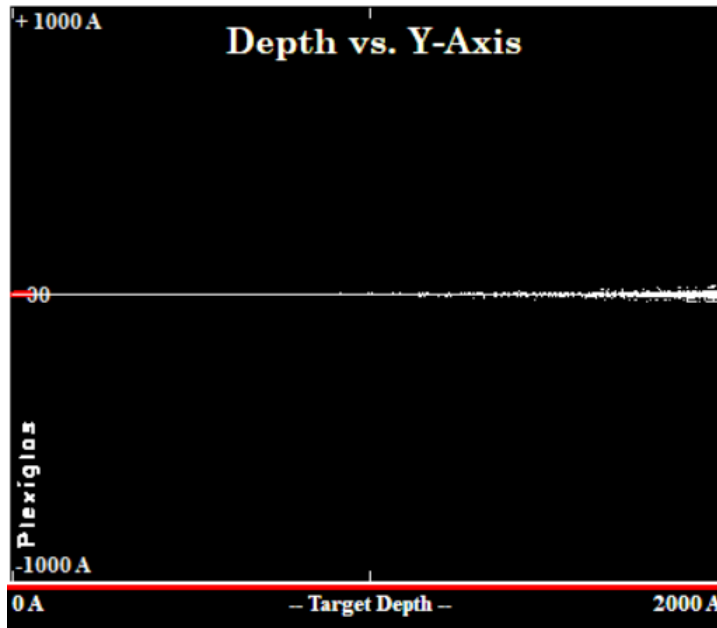


Figure 2-5 A simulation of 750 keV protons traverse through 200 nm thick PMMA (1.19 g/cm³) resist layer.

2.3.3 Beam focusing

1.5 MeV H_2^+ is used to write nano line arrays as the current is large enough to complete writing task within two hours. H_2^+ beam reaching writing chamber have less chromatic aberration since the ions scattered at object apertures are broken-up into individual protons and they can be removed from beam path by the switching magnet [67].

After introducing beam into writing chamber and making it hit on a metal corner of the sample holder, current is measured using a Pico ammeter (rbd 9103 USB Picoammeter) with 0.1 pA sensitivity. For 1.5 MeV H_2^+ , beam current around 2 nA is enough for operators to focus beam down to around 1 μm in spot size by minimizing the dimensions of proton induced fluorescence image on quartz [78]. Operators are suggested to use a new piece of quartz after 5 hours irradiation with

current 2 nA for getting better fluorescence image of proton beam. Operators adjust quadrupole lens current power supplies to achieve smallest fluorescence spot on quartz piece. Three quadrupole lenses affect focusing on both X and Y directions while current of lens 1 and 2 has larger effect on Y direction focusing and current of lens 3 influences X direction focusing to a larger extent, see figure 2-2. Required magnetic fields for beam focusing relates to the magnetic rigidity of a beam. In the expression $\frac{p}{q} = B\rho$ where p is the magnitude of the particle momentum, q is the charge of the particle, B is the magnetic field and ρ is the bending radius of the particle in the magnetic field B , beam with larger magnetic rigidity experience less angular deflection when it travels through a field. Rough focusing is followed by controlling the opening of collimator slits to make the center of collimators coincides with center of beam path. It is observed that the object slits opening and collimator slits opening reduce by a couple of microns after beam heating for half an hour and resulting in slit expansion. To have an accurate estimate of slits opening dimensions, users find the positions at which the slits blocks all the beam (the beam current measured by the picoammeter turns to zero) and enlarge the apertures after the slits are heated by beam for a half to one hour.

Sub-micron focusing is done by mapping proton induced signal, for 20-degree beam line STIM and SEM, when scanning the beam across a resolution standard.

Beam scanning a corner of resolution standard, a metal mesh. Scanning area can be calculated by moving the stage for a certain distance. Comparing the positions of grid edge before and after stage movement correlates pixel numbers with distance.

Scanning area is calculated by multiplying pixel size with total number of pixels in each direction.

To determine the actual beam size, line scans in X and Y directions across the edges of metal bars in the resolution standard are extracted. Gaussian function is used to fit electron emission of grid line scans and FWHM is extracted, defining beam spots in X and Y direction [78]. Levenberg-Marquardt method is used to fit beam intensity curve.

Referencing previous settings on quadrupole lens currents helps in finding initial focus in the rough focusing stage. However, tuning the lens power each time is necessary in order to get beam spot size down to 100 nm because the reproducibility is limited by hysteresis [78].

2.3.4 Beam spot size estimation

Beam spot size depends on the opening of object slits, opening of collimator slits in X and Y directions, demagnification in X and Y of quadrupole lens, alignment of the beam line and working distance between the last lens and the sample plane. Beam broadening originates from angular scattering from slit surfaces, which results in spherical aberration, and loss of energy when beam penetrate through slits edge resulting in chromatic aberration [71]. In order to write nanolines with width close to beam spot sizes, resist surface should be placed at the focal plane. After focusing the beam on metal grid bar, the sample substrate is supposed to be brought to the sample plane as the metal grid bars. Measured with optical microscope, the

height difference between grid bars and substrate has errors at $\pm 1 \mu\text{m}$. According to the apertures to image plane distance (7.6 m) and the demagnifications (857×130 in X and Y direction), the half angle beam divergence is calculated as 0.9 mrad and 0.06 mrad with object apertures opening $8 \mu\text{m} \times 4 \mu\text{m}$. Assuming writing on a flat surface that, height difference between different parts are within a micron, proton beam writing features broadening caused by $\pm 1 \mu\text{m}$ dislocation of substrate in Z direction is $0.9 \text{ nm} \times 0.06 \text{ nm}$ which is negligible. Features broadening also depends on the contrasts of photoresist and deterioration as the resist ages.

Because of the 2mV absolute accuracy of the output DAQ card for the electrostatic scanning system, the scan size should not be larger than $5 \mu\text{m}$ when the output voltage is -10V to 10V in order to ensure the beam spot size measurement accuracy in 1 nm [73]. Micro-channel Plate is an alternative for mapping scattered ions at beam current larger than 20000 protons/ second. Currents of quadrupole lens can be changed at 0.001 A accuracy. Combinations of currents for lens power 1 and 2 are tuned till reaching the best focusing condition.

2-3-pixel width line scans are extracted from the image of ions scattered from the resolution standard and the line scans are integrated to improve count statistics for line fitting. Typical pixel size is $7.8 \text{ nm} \times 7.8 \text{ nm}$ when the scan area is $2 \mu\text{m} \times 2 \mu\text{m}$ over 256×256 pixels array. After mapping the ions scattered and fitting the counts in X and Y direction lines, beam sizes in both directions are gauged by the distances between the two points in the fitted lines, where the signal intensity is 88% and 12% of the maximum [79].

Beam spot size is fitted from ion counts intensity profile after scanning over a single line in X and Y directions respectively over an edge of resolution standard. Applying model for secondary electron scattering, edge enhancement is considered in calculation.

$$F(X_0, f, a) = H_{err} \left[1 + \operatorname{erf} \left(\frac{2\sqrt{\ln(2)}}{f} (a - X_0) \right) \right] \\ + H_{gau} \left[\exp \left(-\frac{\ln(16)}{f^2} (a - X_0)^2 \right) \right]$$

In the model, f is beam's FWHM. a is position of the resolution standard grid edge. The term containing H_{gau} correlates to the distortion of the output due to edge enhancement. Detecting scattered ions using STIM or dealing with beam profiles without visible edge enhancement phenomenon, this term is set to zero. [75]

Horizontal beam profile exhibits smaller spot size mainly due to lower demagnification in vertical direction. Other points of considerations are: increased aberrations, slit scattering and stray magnetic fields influencing beam in one direction.

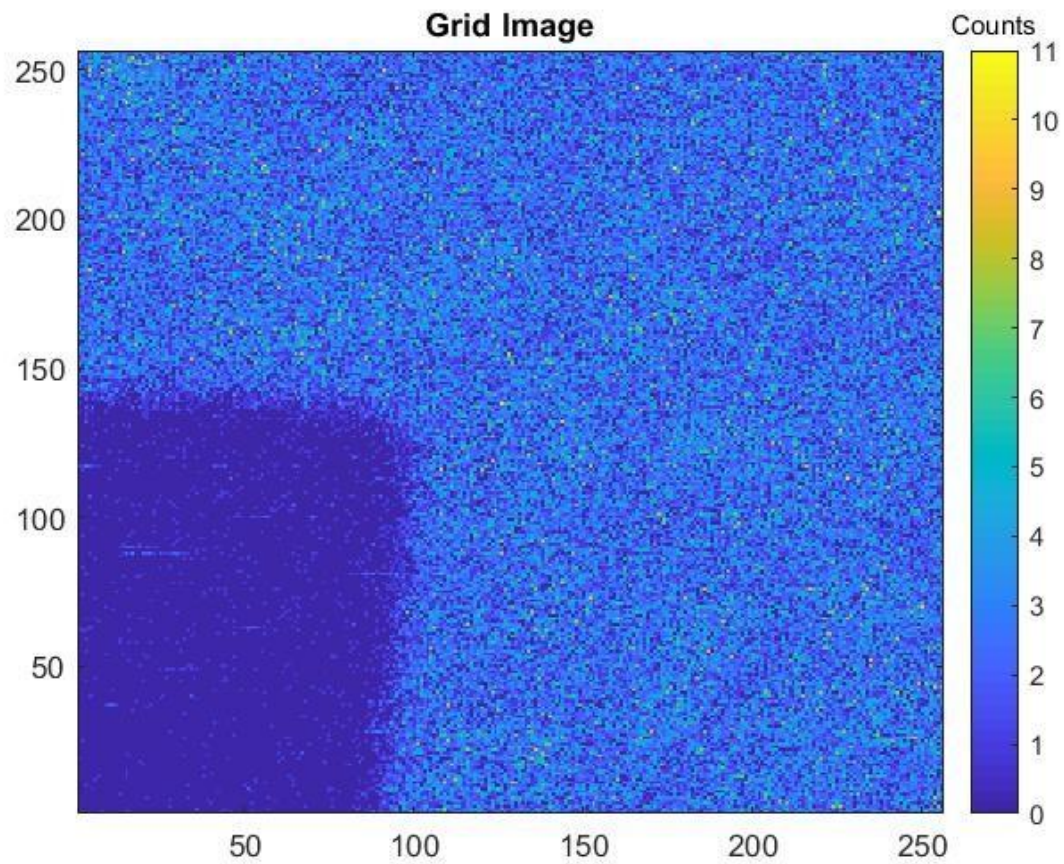


Figure 2-6 Intensity map of protons scattered from a corner of a resolution standard by scanning the beam at 2 microns range.

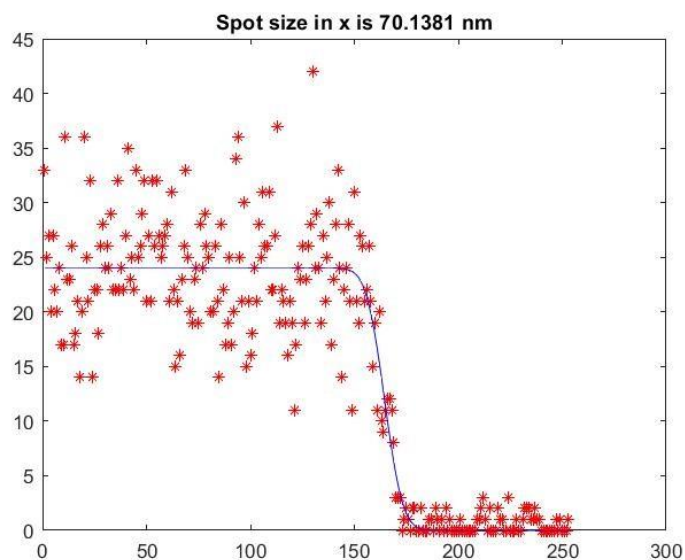


Figure 2-7 Proton counts at X direction line and fitted curve. The pixel size is 7.8 nm. FWHM of the curve is defined as spot size in X direction, which is 70.1 ± 7.8 nm.

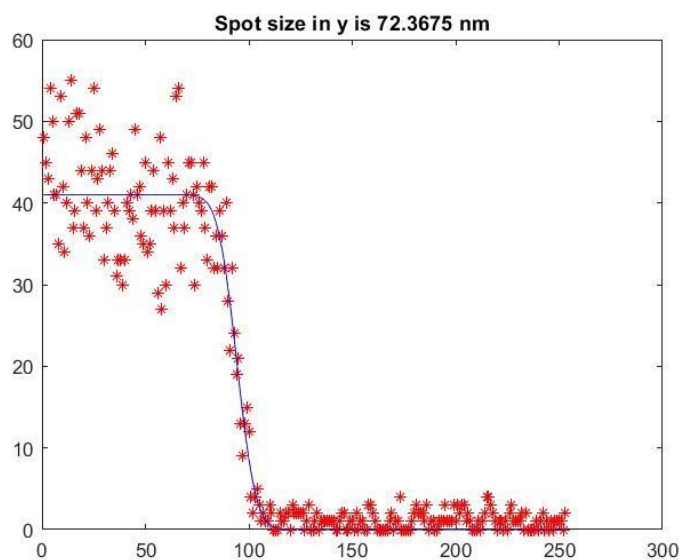


Figure 2-8 Proton counts at an Y direction line and fitted curve. The pixel size is 7.8 nm. FWHM of the curve is defined as spot size in Y direction, which is 72.4 ± 7.8 nm.

2.3.5 Current measurement

Beam current can be measured by pin diode mounted intercepting the beam path behind the sample plane. It is found that ions are not fully counted when the count rate is larger than 1000 counts per second due to the update time limit of the main amplifier. Pin diode is moved to on-axis position and ions hit detector surface without scattering. Object slits and collimator slits are adjusted to certain sizes with which the beam count rate less than 1000 Hz and the count rate is noted down. By opening objects slits and collimator slits further, pin diode detector is moved away from beam axis to prevent it from being damaged by large current. The beam current is calibrated taking a ratio between on and off-axis STIM.

2.3.6 Programming writing path

Scanning voltage is programmed to write lines with different widths. +10 V to -10 V with absolute accuracy 2 mV can be applied to the electrostatic scanning system. Beam control and scanning system utilizes National Instruments M-Series PCI/PXI 6259 DAQ card, which allows 1MHz pixel update time scan speed imaging [73].

Proton writing can be done by moving of sample stage relative to the beam path, combining with beam scanning by applying electric field to scan plates. By moving the sample stage with closed loop control of 4 nm accuracy at a range of 20×20 mm², patterns of millimeter dimensions can be formed in resist. Beam can be scanned orthogonally to the direction of stage moving, for example of writing tapered nanochannels array in XR1541, the stage is moved in Y direction for 60 μ m while the beam is scanned in X direction for 400 nm and gradually reduced to

0 to write channels with tapered ends. Without beam scanning in the orthogonal direction of stage movement, lines are written on resist with width determined by the beam spot size and exposure dose. The inputs for a writing by stage movement are stage moving direction (X or Y), coordinates of stage starting and end positions, amplifier update frequency and scan voltage in the direction orthogonal to stage movement. The electrostatic scanning is done orthogonally to the stage movement. Fast stage moving may result in un-exposed region along the beam scan path. Stitching errors should be considered when writing continuous features with more than one writing commands. Stage may be hundreds of nanometers away from the previous positions which indicated by same coordinates. In the example of writing tapered nanochannels in PMMA resist, the stage moved 10 μm in Y direction for writing a wide channel and stepped back for 3 μm before writing the next narrower channel to encounter the possible positioning error in Y direction.

Table 2-1. Parameters set for writing a PMMA nanochannel by moving the sample stage in one direction.

Stage direction	Y	Stage velocity	0.00054 (mm/s)
Starting position X	-7.06 (mm)	Starting position Y	-2.308 (mm)
Final position Y	-2.158 (mm)	Scanning voltage	0
Line dose	6.25×10^7 ions/mm	Stage movement length	0.15 mm
Channel width (estimated using beam spot size)	0.05 μm	Area to be written	$7.5 \times 10^6 \text{ mm}^2$

Ions needed	9.375×10^6 ions	Ion number needed per second	2.71×10^5 #/second
Writing time needed per channel	35 seconds	Stage speed	4.34×10^{-3} mm/s

Another mode of beam writing can be achieved by controlling beam scanning in X and Y directions by electric field. The patterns can be in monochromatic *bitmap* or *ascii* file format and converted to *epl* file format by the *Ionutils* software, which was developed for the proton beam writing [80]. The *epl* files contains X and Y position of the beam and blanking level, describing the beam paths that form the designed patterns and the paths during which the beam should be blanked. During file conversions, the *epl* file resolution can be set and thus, the beam scan is to expose or blank certain numbers of pixels, for example 4096×4096 pixels which is supported by maximum 16-bit National Instruments M-Series PCI/PXI 6259 DAQ card. In our system it has effective 13-bit resolution [73]. Pixel size in X and Y directions are calculated by beam scan area dividing with resolution. Beam dwell time for each pixel is: dose (nC/mm^2) \times one-pixel area (mm^2) / beam current (nC/second). Beam update frequency is the reciprocal of the beam dwell time, limited by the slew rate of the scanning amplifier. The number of pixels that need to be exposed and blanked are shown in the software *Ionutils*. Thus, the total writing time can be estimated as the product of pixel numbers and beam dwell time for one pixel. The center coordinates of the pattern (X and Y), frequency, largest scan voltages in X and Y directions together with the *epl* file name are inputs for a beam

scan writing command. Beam spot size should be larger than the pattern map pixel size so that exposed area overlaps and form continuous structures. In the example shown below, the beam is scanned in a arrange of $74\text{ }\mu\text{m} \times 71\text{ }\mu\text{m}$ in X and Y directions with the beam size $5 \times 10^{-9}\text{ mm}^2$ and the pixel area $3 \times 10^{-10}\text{ mm}^2$. The dose applied in the experiment is estimated as total amount of ions applied to write a line. An example of parameters used in 1.5 MeV H_2^+ writing on XR1541 resist by beam scanning is listed below.

Table 2-2. Parameters for a beam scan writing on XR1541 resist.

Pattern resolution	4096×4096 pixels	Scan area	$74 \times 71\text{ }\mu\text{m}^2$
Pixel area	$3.13 \times 10^{-10}\text{ mm}^2$	Line dose	1.75×10^9 ions/mm
Ion count rate	3.11×10^6 counts/sec	Current	$4.98 \times 10^{-4}\text{ nC/sec}$
Dwell time per pixel	$1.26 \times 10^{-4}\text{ sec}$	Frequency	7954 Hz
Pixels to be exposed	3604990	Pixels to be blanked	12321861
Total number of pixels	15926851	Time for writing	2002 seconds

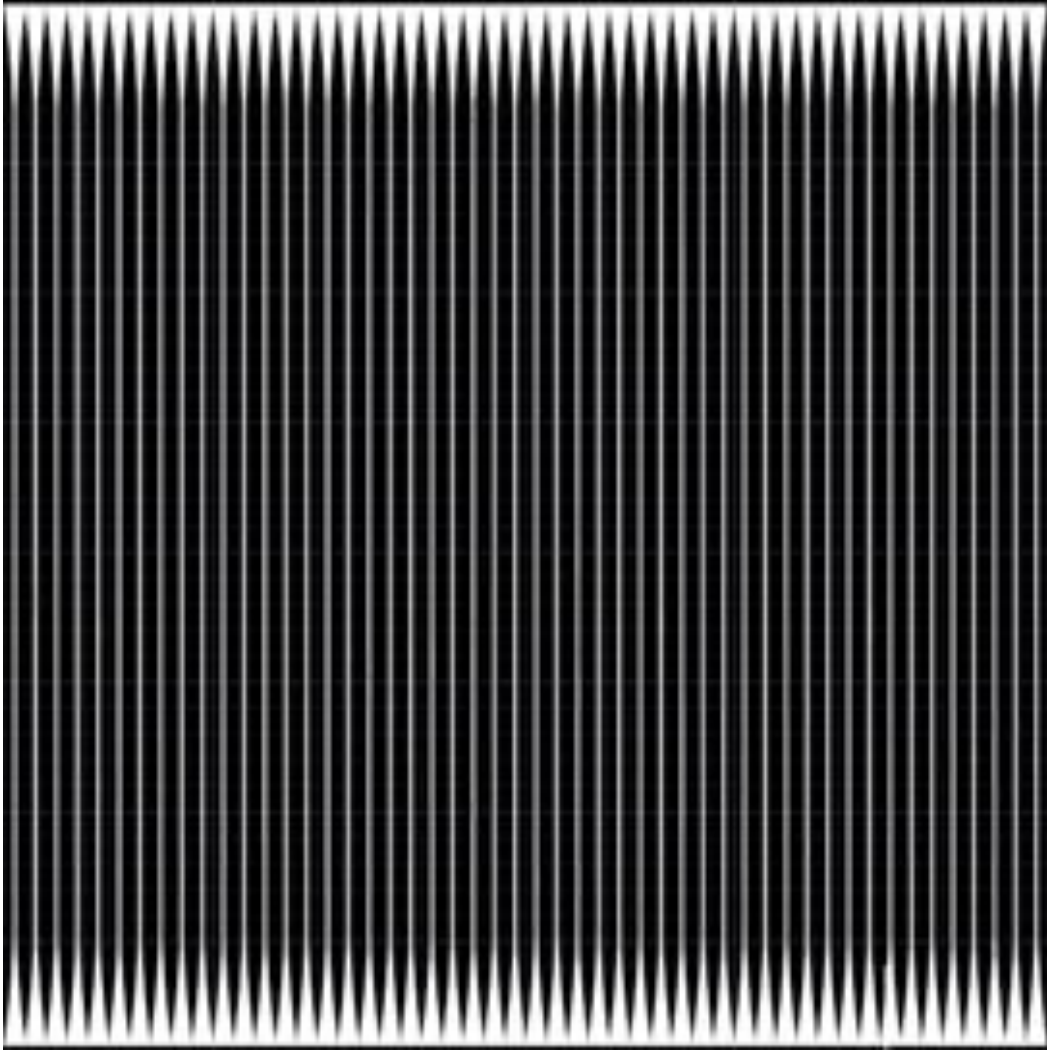


Figure 2-9 Drawing of 50 tapered nanochannels which are written on HSQ resist by scanning 1.5 MeV hydrogen molecular beam in X and Y directions.

Figures can also be programmed as *emc* file that indicating the resolution of figure, shapes in the figure such as rectangles, circles, spiral squares and spiral circles, center coordinates of each shape. Beam path can be controlled in the *emc* file to avoid unwanted resist exposure at critical edges of the shapes that degrade the edge smoothness [80].

Chapter 3 Nanofluidic Chip Fabrication

3.1 Overview of fabrication methods

3.1.1 Nanopatterning methods

Many fabrication methods have been developed to pattern elastomer and thermoplastic materials, forming nanoslits with one dimension below 100 nm or nanochannels featuring nanosized cross sections [81][82]. Electron beam, focused ion beam and femtosecond laser beams are commonly used to fabricate channels featuring sub-micron sized cross sections [83][84][85]. Among direct writing techniques, proton beam writing shows superior characteristics in forming high aspect ratio nanosized patterns on resist with straight and smooth side walls [86][87]. Combining photoresist development with etching techniques on silicon and glass substrates, various nanostructures are formed and developed for applications in nanofluidics. As an alternative to brittle glass, fused silica and silicon-based fluidic devices which require dedicated nanofabrication facilities [88][22][89], polymers have advantages as nanofluidic chips material [90]. Moreover, simple low-cost and high-throughput replications via nanoimprinting lithography (NIL) [91] and thermal sealing methods make polymer nanofluidics well suited for a diverse range of applications [92][66]. NIL has been widely used in nanofluidic chips fabrication of multi-level structures over large areas in a cheap and fast mode [93][94]. During the development of nanoimprint, stamps made of hierarchically fabricated in SiO_2 or Si using RIE [95][96], metal mold for imprinting on thermoplastic substrates [6] or quartz and glass stamps through etching are widely

used [97]. Nano trenches are also formed using sacrificial material wet etching and thermal degradable templates [98]. Silicon microchannel and nanochannel chips are sealed by Pyrex using conventional anodic bonding [95] or shadow sputtering deposition [88], sacrificial polymers [99] and modified NIL process [97]. A thin layer silicon oxide is grown on silicon nanochannel chips at 1000 °C for 2.5 hours to isolate electricity as well as forming a hydrophilic surface for fluidic injection. Metal is coated on top cover around the inlet holes which are created by femtosecond laser ablation.

3.1.2 Lab on a chip fabrication

Direct writing on PMMA using focused proton beam on Kapton (Kapton® HN from DuPont) substrate and capping with PMMA sheet (PLEXIGLAS®) forming enclosed nanochannels method was introduced by Shao et al [100]. As illustrated in figure 3-1, PMMA (formerly Microchem Corp.) 1-10 µm is spincoated on a 50 µm thick Kapton film, patterned using proton beam writing and bonded to a flat PMMA sheet. Kapton substrate is peeled off and another flat uniform PMMA sheet is bonded at the bottom forming a substrate. This process is based on the strength and flexible qualities of Kapton as well as the fact that the bond strength of Kapton-PMMA is smaller than the bond strength between two properly bonded PMMA sheets. During thermal bonding, the Kapton film also promotes uniformity of contact pressure avoiding warps and breakages of structures. 200 nm wide and 2 µm deep channels cross section are formed. The method is also used to fabricate 100 nm wide × 2 µm deep nanochannels connected with micro channels and reservoirs [87].

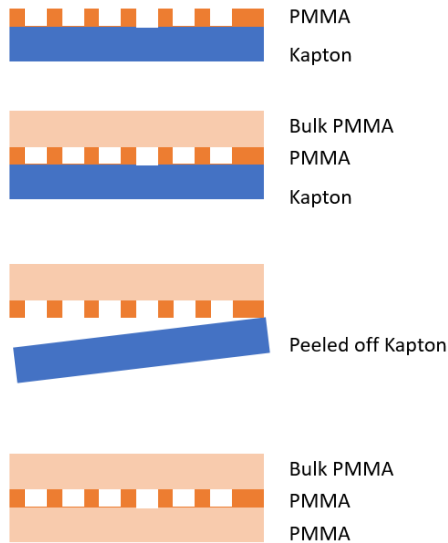


Figure 3-1 Enclosed PMMA chip using Kapton as substrate.

There is a single step irradiation process making buried tunnels using 3 MeV proton beam reported by B.Rout etc. [51]. Micro size buried channels form at bulk PMMA where the energetic proton penetrates and stop inside the block and exhibit enhanced end-of-range damage. Ion fluence and chemical developing process are carefully calibrated to allow only the volume at the end of penetrating path to be removed but not the polymer on the trajectory. Experiments about the fluence forming end-of-range damage in 3 mm thick PMMA is carried out with 2 MeV proton as shown in figure 3-2. Another proton beam writing on PMMA was done using 1.5 MeV H_2^+ ions with dose range from 1 to 6 nC/mm² as shown in figure 3-3. Lines were written on 3 mm thick PMMA and developed in IPA:DI = 7:3 solution at room temperature for 4 hours. Two sets of lines cross each other and sits in between marker lines written with 120 nC/mm² fluence. 75 μm \times 150 μm

reservoirs connect to terminals of the lines serving as inlet of developers. It is concluded that with 1.5 MeV H_2^+ ions the buried channel structures can be formed with irradiation dose 2 to 6 nC/mm².

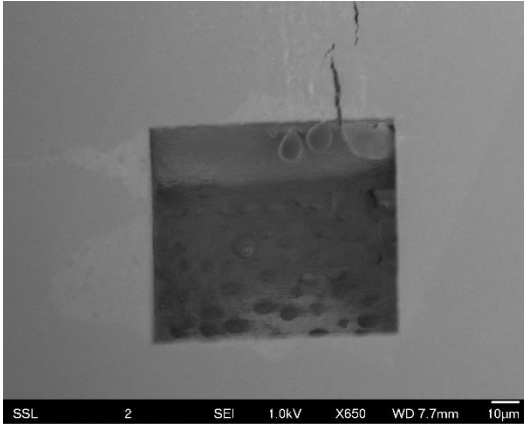


Figure 3-2 2 MeV proton writing lines connecting of a square reservoir showing end-of-range damage to bulk PMMA.

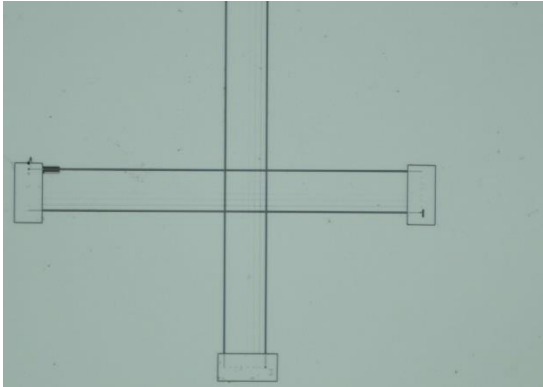


Figure 3-3 Optical image of 1.5 MeV molecular hydrogen ions writing on bulk PMMA forming buried channels.

Besides direct writing methods, lines pattern can also be formed by masked lithography. PMMA A2 is coated on silicon substrate with spin speed 1000 rpm, giving the thickness 89.3 nm, calibrated by AFM (SPM-Bruker Dimension® Icon™). A nickel mask carrying nanolines patterns is placed on top of the resist, allowing energetic ions reaching the resist through the patterned slits. Dose used

for the irradiation is 2.5×10^{13} ions/cm² (40 nC/mm²). As shown in figure 3-4, hundreds nanometer size patterns can be made through broad beam irradiation, providing a fast solution for nanopatterning. However, patterned masks need to be made in advance. Gaps between masks and resist layer enlarge irradiation area and thus, enlarge nanopatterns. Flat and clean mask and resist surfaces are also required.

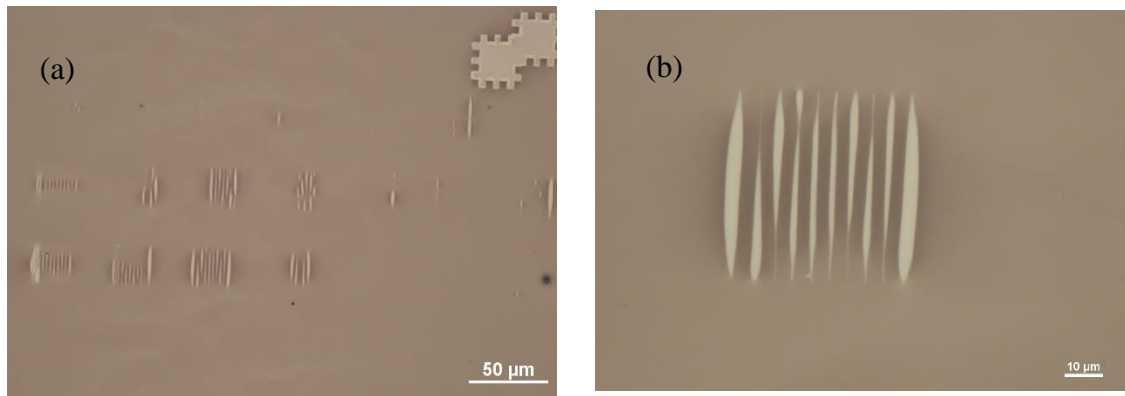


Figure 3-4 Optical images of PMMA patterns formed by irradiating 100 keV hydrogen molecular ions over masked PMMA resist.

3.1.3 Pattern transfer from molds, stamps to nanoimprinted chips

In this project, nanopatterning is implemented with the production of molds and stamps for subsequent nanoimprinting of nanofluidic lab on chip devices. Figure 3-5 is the schematic illustration. Here, channels with nanoscale cross sections are replicated from photoresists which are patterned by proton beam for nanoscale features and laser writing for micron sized features. PMMA and HSQ are high resolution resist [101][50] and they are used to form the desired network of channels featuring nanoscale cross section and a typical length of 10s up to 100 μm in length. In a subsequent step these molds are transferred into rigid molds such as OrmoStamp. These hard molds can then be used in a nanoreplication step via

casting or nanoimprinting to form desired nanopatterns in polymer materials with high fidelity. Finally, these polymer materials are sealed via a bonding process to form high quality nanofluidic LOC devices. Details of the fabrication procedures will be discussed in the following sections.

OrmoStamp (Micro resist technology GmbH) is a UV patternable inorganic-organic hybrid polymer, which can be used as nanopatterned stamp for nanoimprinting and PDMS casting. Ormostamp enables patterns in mm, μm and nm dimensions to be transferred in one-time casting. However higher temperatures applied during imprinting limit the lifetime of OrmoStamp. Diamond-like-carbon coating can be applied on Ormostamps to enhance the durability of the stamps. Patterns can be transferred from resist molds like PMMA and HSQ molds to Ormostamps (Micro Resist technology GmbH) with high fidelity on resolutions down to tens of nanometers. Thus, it is a suitable candidate for molds of nanochannels. The OrmoStamp mold was reported to be used in making 30 nm nanochannels direct imprinting by Irene Fernandez-Cuesta etc. and also tested on transferring nano ridges and channels to PMMA [102][103]. Optical transparency of OrmoStamp make it suitable for UV-NIL. Crosslinked OrmoStamp is mechanically hard and high-temperature durable, which make it a candidate as mold for thermal imprinting. OrmoStamp is also reported to be used as fluidic chip devices because it is stable in high temperature, hydrophilic after 1 min UV-Ozone treatment and inert.

Nickel stamps can also be used in nanoimprinting, capable to transfer sub-100 nm high aspect ratio features to polymer material, the stamps have a long lifetime. To

make a nickel stamp, a silicon substrate is sputtered with 30 nm Cr and 60 nm Au as nickel electroplating seed layer. Ni can also be electroplated on a resist master mold by a metal-on-metal process. 1.5 nm Ti is coated as electrically conductive layer on top of the resist master mold for plating the first nickel stamp, which carries reversed patterns [104]. The first nickel stamp is immersed in 30 % hydrogen peroxide for 90 seconds, forming a layer of oxide before second time Ni plating [40]. The nickel mold with cross section dimensions $4.5\ \mu\text{m} \times 4\ \mu\text{m}$ microchannel and $110\ \text{nm} \times 800\ \text{nm}$ nanochannel is replicated through PDMS casting followed by bonding to a glass substrate to produce PDMS LOC devices. These PDMS LOC devices are used to image fluorescence of YOYO-1 stained single T4 GT7 DNA [41].

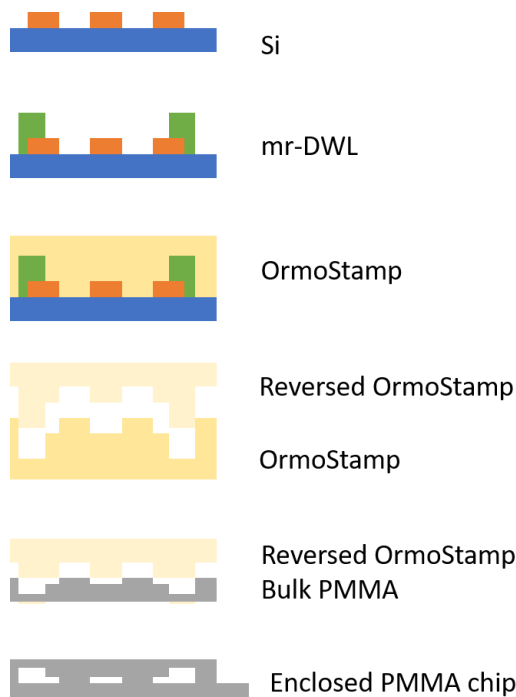


Figure 3-5 A schematic illustration of making enclosed PMMA chip by making resist master mold, Ormostamp, imprinting on PMMA and bonding method.

3.2 Design and fabrication requirements

Polymer materials like polydimethylsiloxane (PDMS) [105][106], poly(methylmethacrylate) (PMMA), polycarbonate (PC) and cyclic olefin copolymer (COC) are commonly used to replicate nanofluidic lab on chip devices. X-PDMS is a stiffer variation of PDMS and has been shown to be a viable candidate for nanofluidic lab on chip reproduction [107][108]. The surface chemistry can be modified to facilitate various applications. Excellent optical properties and biocompatibility make polymer fluidic chips an attractive choice for several biological fluorescence experiments as well as extreme pH condition [6]. Optical transparency, biocompatibility, low cost and fast production are requirements for LOC devices to be compatible with biomedical research. Among the polymers, X-

PDMS, PDMS and PMMA exhibit relatively low auto fluorescence levels compared to other materials used for fluidic chips such as COC [109] which is a critical characteristics for single molecule detection. Patterns can be transferred from hard molds to various polymer materials followed by machining of essential fluidic chip structures such as nanochannels and fluid reservoirs. Micron-sized channels are designed to facilitate fluid flow from inlet and outlet reservoirs to the nanochannels. My design of microchannels is shown in figure 3-6, four reservoirs with diameter 1 mm are used for easy fluid handling.

Due to relatively low Young's modulus of polymers, the aspect ratio (height / width of a nanochannel) of a fluidic circuit has to be chosen carefully. PMMA's Young's modulus is 1.8-3.1 GPa while it is 2.3 MPA for PDMS and 20-80 MPa for X-PDMS [107][108]. Since PDMS has the lowest Young's modulus it is not rigid enough to support very fine nanochannels cross sections. X-PDMS and PMMA are therefore more preferred to as they support channels with cross sections even below $50 \times 50 \text{ nm}^2$. As PMMA has the largest Young's modulus of the 3 it can support nanochannels with an aspect ratio up to 10, whereas PDMS can only support an aspect ratio up to 3 for PDMS. PMMA is therefore more versatile and can accommodate a larger height to width ratio.

Nanochannels are designed with tapered ends (figure 3-7) to facilitate loading of DNA molecules [6]. With gradually evolving degree of confinement, DNA molecules can be load to nanochannels from microchannels. Other methods such as introducing nanosized obstacles [110] and micropost arrays [95] in front of nanochannels to pre-stretch the molecules also helps in reducing the big entropic

gap between micron-size and nano-size channels. Proton beam sweeps in X direction for 400 nm at starting of a line writing task and gradually reduces to 80 nm scanning. The tapered part is 60 μm long. A 150 μm long line is written by beam without scanning in X direction but only the stage is moved in Y direction. The final width of nanochannels depend on the beam spot size, developing procedures, stamp fabrication and polymer casting procedures which are calibrated to transfer structures without defects and widening. 175 μm PMMA sheet (PLEXIGLAS®) is imprinted with nanochannel patterns to ensure the interested particles are positioned within fluorescence microscope objective working range. Accurate fabrication of enclosed nano channels is critical for DNA single molecule analysis. Nanochannel with dimension close to the persistence length of double stranded (ds)DNA (~ 50 nm) is of great value for research related to single DNA molecule genome mapping.

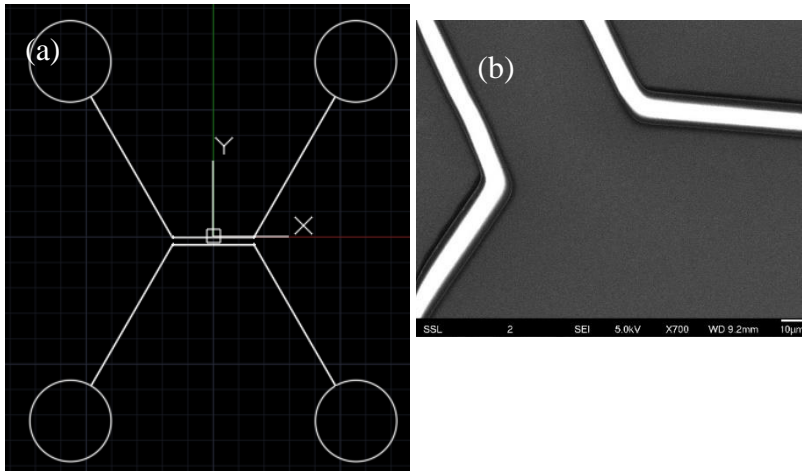


Figure 3-6 (a) Design of microchannels and reservoirs in CAD. (b) SEM image of a mr_DWL microchannel master mold.

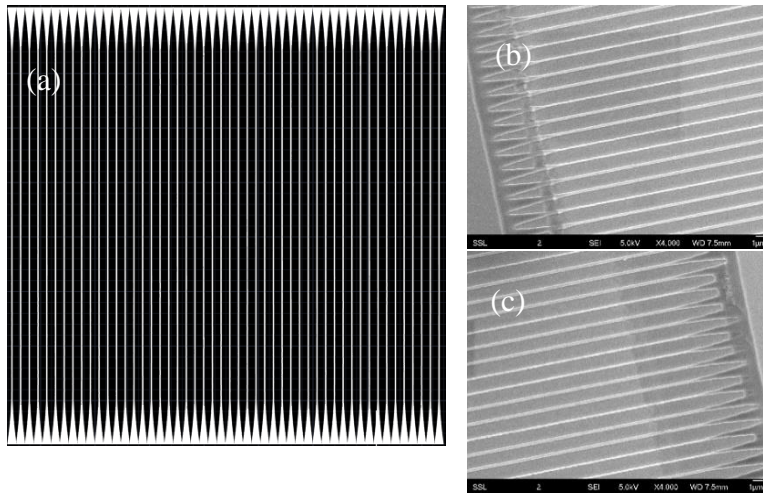


Figure 3-7 (a) Design of nanochannel array in CAD. (b) and (c) SEM image of HSQ master mold of tapered end of nanochannels.

3.3 Mold making

3.3.1 Resist molds

Photoresist is spin coated on a silicon substrate and prebaked to form a uniform layer with a thickness of ~ 100 nm to several micrometers depending on the specific section of the fluidic circuit that is being prepared. Thickness of coated resist varies with polymer types, solvent content, and coating procedures. Calibration of resist thickness is necessary to accurately control channel dimensions. Focused proton beam excites electrons in the resist and these excited electrons induce polymer chain scission or crosslinking. After resist development, nanosized ridges or grooves form on the substrate, depending whether a negative or positive tone resist is used, respectively. Patterns can be formed in photoresist by proton beam writing.

PMMA resist mold

Silicon wafer can be baked to be dehumidified at 100°C for 5 mins. A drop of PMMA (formerly Microchem Corp.) is spread on the silicon wafer and spun at 500 rpm for 5 seconds, 2000 rpm for 20 seconds and 4000 rpm for 45 seconds. It is prebaked at 180 °C for 80 seconds before proton beam exposure. After resist developing, the thickness of the grooves is measured to be 72 nm.

As shown in figure 3-8 and figure 3-9, lines are written on spin coated PMMA layer (PMMA 495k A2, formerly Microchem Corp.). After developing in isopropyl alcohol (IPA)-water (7:3 by volume) mixture, grooves with cross sectional dimensions 72 nm × 200 nm (height × width) are formed (figure 3-10). The PMMA master mold is coated with 2 nm diamond-like-carbon by Filtered Cathod Vacuum Arc (Nanofilm Technologies Internatioanl Pte Ltd) and used for Ormostamp casting. There are some imperfections observed in figure 3-9, which is possibly due to minor irregularity in stage motion.

HSQ resist mold

HSQ (XR1541-002, Dow corning) is kept in fridge at 0-4 °C. It is spin coated on silicon wafer at 4000 rpm for 45 seconds and pre-baked on a 150 °C hot plate for 120 seconds. It is reported that 80 nm thick HSQ can be formed on silicon substrate while minimum dose required for cross-linking and thickness of resist layer vary batch to batch [94]. A calibration in thickness of the XR1541 resist spun on silicon substrate is described below and reporting a layer thickness around 132 nm by spin coating speed of 4000 rpm (figure 3-11). Tapered nanochannels are written by 1.5 MeV H₂⁺ beam (figure 3-12, figure 3-13) scanning in X and Y directions. Details

are discussed in section 2.3.6. There are some imperfections shown in figure 3-13 and figure 3-23 which is due to beam tuning.

mr_DWL resist mold

Resist mr_DWL (Micro resist technology GmbH) is spun on silicon substrate at a speed of 3000 rpm. Prebake is done at 50 °C for 2 mins and at 90 °C for 4 mins. Thickness of the developed mr_DWL ridges is characterized with AFM to be 5 μm (figure 3-14, figure 3-15). To make double-layer resist master mold, mr-DWL (Micro Resist Technology, GmbH) is spin coated on top of XR1541 resist master mold at a speed of 3000 rpm. The microchannel patterns are written to be connected with nanochannels by laser writing (μPG101 , Heidelberg instruments). Post-exposure bake is at 50 °C for 2 mins and 90 °C for 5 mins. Resist mr-DWL is developed at mr-Dev600 for 5 mins. The optical image shows the microlines pattern connects with XR1541 nanolines (figure 3-16).

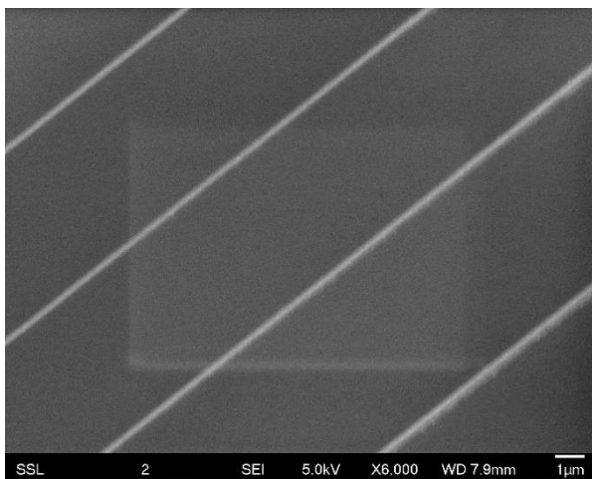


Figure 3-8 SEM images of PMMA nanochannels on silicon substrate of dimension 72×120 nm (depth \times width) written by 1.5 MeV hydrogen molecular beam with stage movement in Y direction.

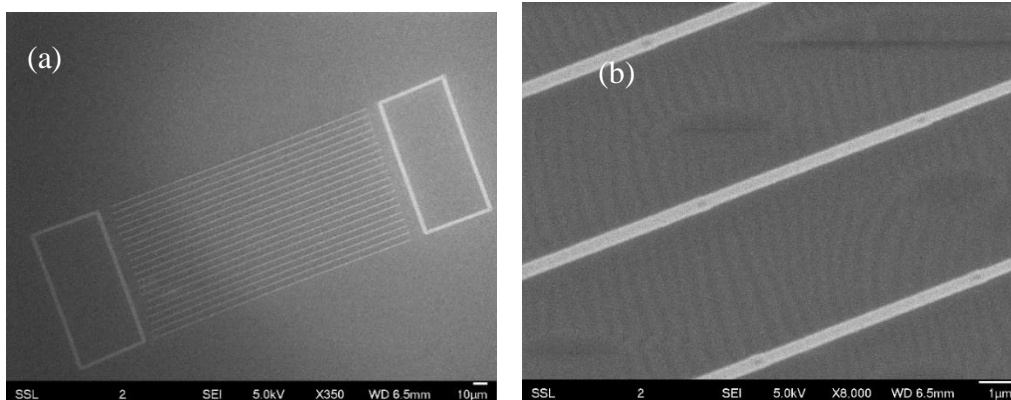


Figure 3-9 SEM images of PMMA spincoated on Si wafer and patterned with proton beam writing. (a) Nanochannel arrays with two square markers; (b) higher magnification image. The channels are of dimension $72 \text{ nm} \times 200 \text{ nm}$ (depth \times width). The patterns are written by 1.5 MeV hydrogen molecular beam with stage movement in Y direction.

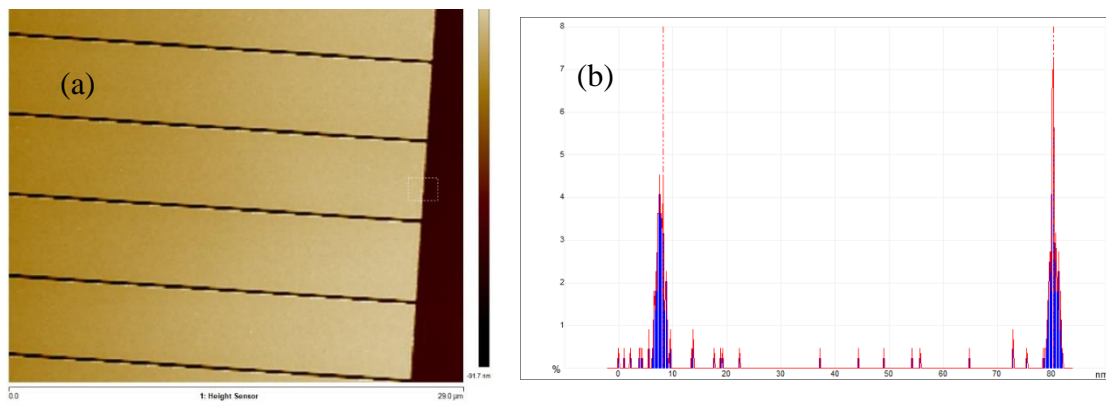


Figure 3-10 (a) Height profile of PMMA master mold containing nanochannel patterns from AFM. (b) Height profile histogram showing thickness of PMMA is around 72 nm.

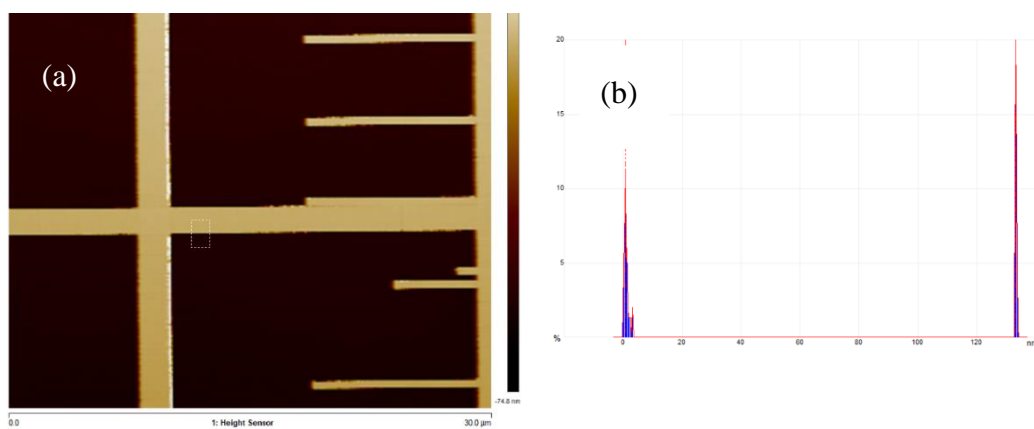


Figure 3-11 High profile from AFM on HSQ microchannel and nanochannel. (a) Height profile mapping containing microsize and nanosize channels. (b) Histogram on an edge of microchannel indicating the thickness of HSQ layer is around 132 nm.

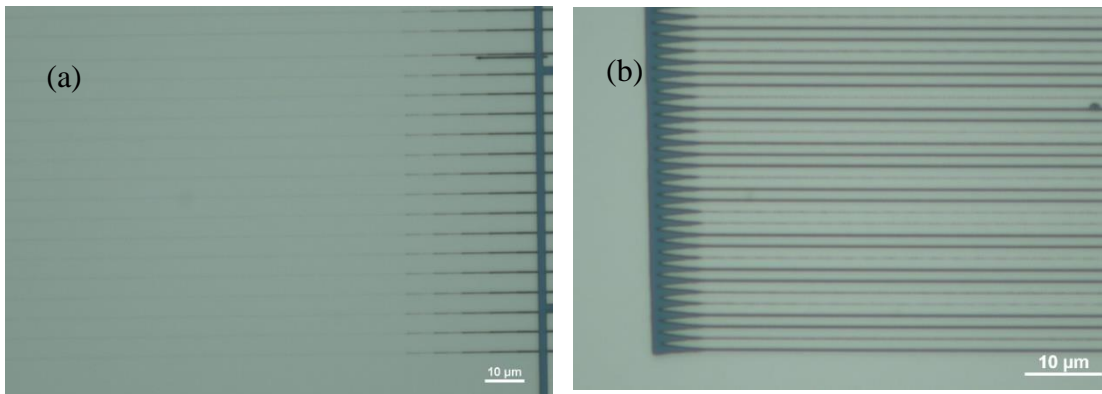


Figure 3-12 Optical images of nanolines formed by PBW on 132 nm thick XR-1541 resist. (a) Tapered lines were formed by sample stage movement and beam scanning in the orthogonal direction. (b) A nanolines array is formed by beam scanning.

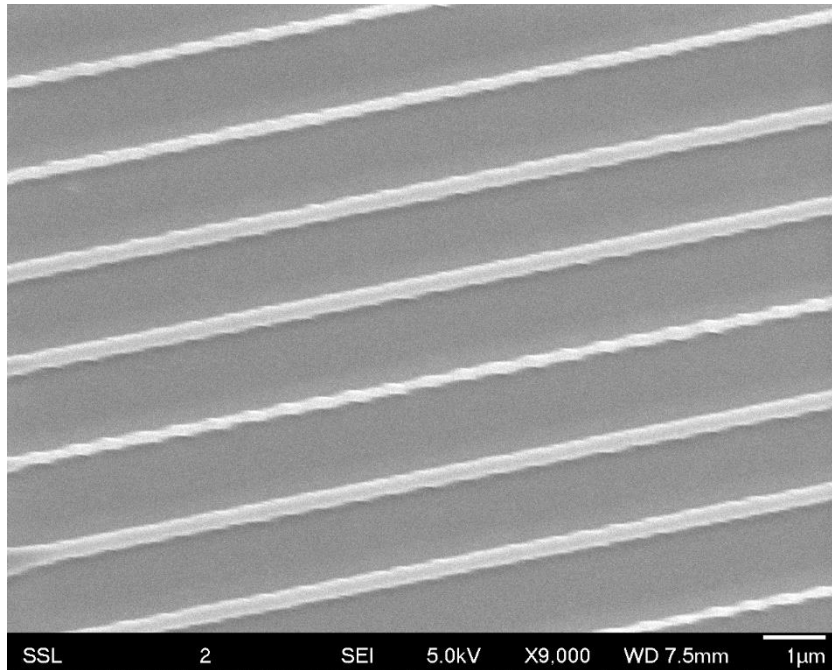


Figure 3-13 SEM image of HSQ lines written by proton beam writing with dimension 132 nm \times 231 nm (height \times width). The lines are written by 1.5 MeV hydrogen molecular beam with beam scanning in X and Y directions.

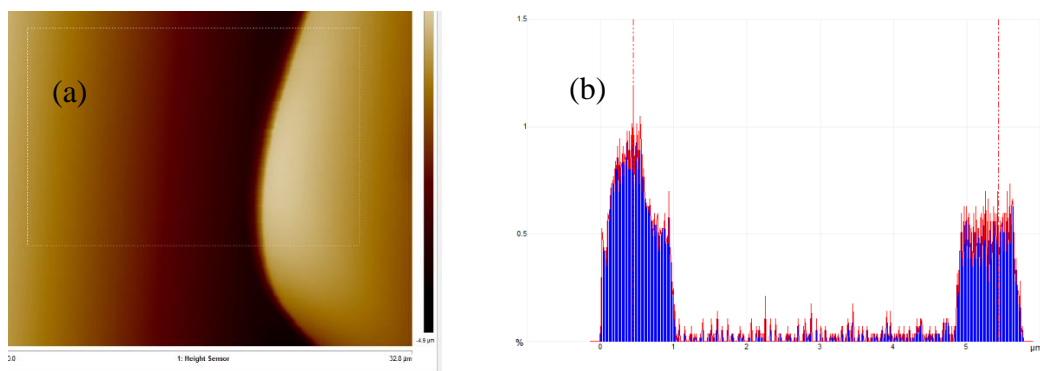


Figure 3-14 (a) AFM characterisation of mr-DWL master mold with microchannel pattern. (b) Peak-to-peak distance showing the thickness of the DWL wall is around 5 μm .

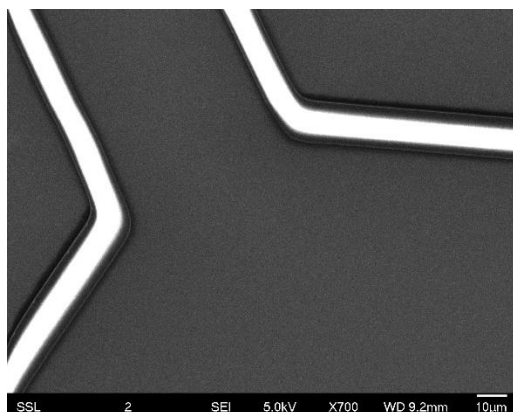


Figure 3-15 SEM image of mr-DWL microchannels with dimension 5 $\mu\text{m} \times 7.3 \mu\text{m}$ (height \times width).

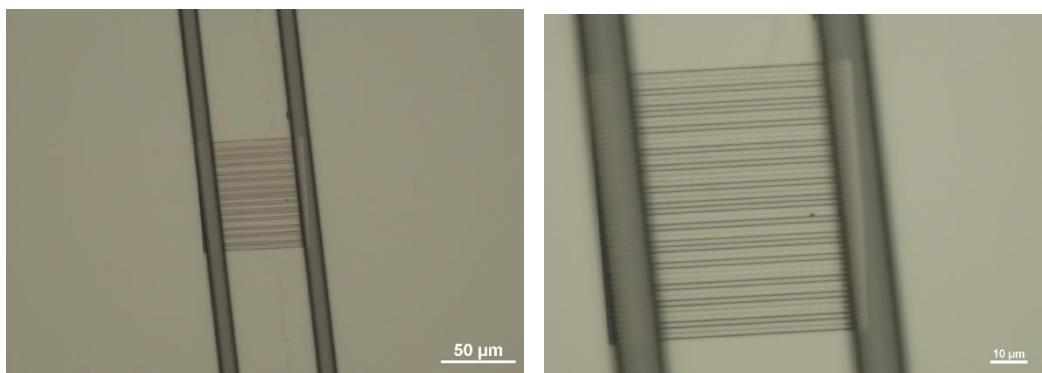


Figure 3-16 Optical images of double-layer master resist containing XR1541 nanolines and mr-DWL microlines.

3.3.2 Ormostamp fabrication

Glass slide cleaning

Take a clean glass slide and clean it with acetone and IPA if necessary. Plasma treatment (Harrick, Ossining, NY) at 300 mTorr pressure, 18W(High) power for 30 seconds. It improves the hydrophilicity of the glass slide, which will be used as the substrate of OrmoStamp [111].

Ormoprime 08 coating

Spincoat OrmoPrime 08 (Micro Resist technology GmbH) on the cleaned glass slide at 4000rpm for 1 minute, followed by soft baking at 150 °C for 5 minutes. This step improves subsequent OrmoStamp adhesion with the glass slide.

Teflon or diamond-like-carbon coating

Teflon coating procedure: 2000 rpm for 30 seconds. However, teflon layer (AF[®] 1600) should be cured for 12 hours before using, which increases fabrication period. Diamond Like Carbon coating (Filtered Cathod Vacuum Arc, Nanofilm Technologies International Pte Ltd) procedure: 20 Amp. 5 mins coating or 31 Amp for 80 seconds gives around 2 nm DLC layer on the master mold. This step assists in demoulding because diamond-like-carbon layer exhibits anti-adhesive property. Anti-stick coating layer should be carefully controlled and kept thin to avoid aggregate in corners of structures to affect the structure resolution. In the DNA nanofluidic experiments, no differences are observed if Teflon is applied or a 2 nm DLC film is applied via Filtered Cathodic Vacuum Arc deposition (Nanofilm Technologies International Pte Ltd) as anti-stick layer.

Ormstamp spread

Spread one drop (<0.5 ml) OrmoStamp (Micro Resist technology GmbH) on the master mold, which is coated with Teflon or DLC. Excessive Ormostamp may cause bump on the master mold and difficulty in demoulding.

Cover Ormostamp with glass slide

Cover the OrmoStamp with the glass slide which is coated with OrmoPrime 08 (Micro Resist technology GmbH). Place the glass slide from one end of the droplet to minimize air pocket between. Leave the sample for 5 minutes.

UV curing

Place the sample under 365nm UV lamp for 5 minutes.

Demolding

Peel glass slide off from the edge. Blade can be used to open a gap between casted Ormostamp and the masterpiece to aid demolding.

Coating with DLC

Diamond-like-carbon is coated with Filtered Cathodic Vacuum Arc deposition (Nanofilm Technologies International Pte Ltd). This step helps to enhance the durability of Ormostamp during imprinting in high temperature and pressure.

Microchannel patterned on spin coated DWL_5 (Micro Resist Technology, GmbH) photoresist using laser writer (μ PG101, Heidelberg instrument) was coated with diamond-like-carbon (Filtered Cathod Vacuum Arc, Nanofilm Technologies International Pte Ltd) and used for making Ormostamp and reversed pattern Ormostamp. The Ormostamp fabrication procedure discussed above is summarized in figure 3-17. Figure 3-18, figure 3-19 and figure 3-20 show AFM images of Ormostamps casted from PMMA resist molds which are discussed in section 3.3.1. The height variations are due to surface roughness. Figure 3-21 and figure 3-22 are optical microscopy images of the Ormostamps casted from PMMA resist molds. Figure 3-23 is a SEM image of an Ormostamp casted from a HSQ resist mold which are discussed in section 3.3.1, showing high fidelity in dimensions during patterns transfer from resist molds to Ormostamps.

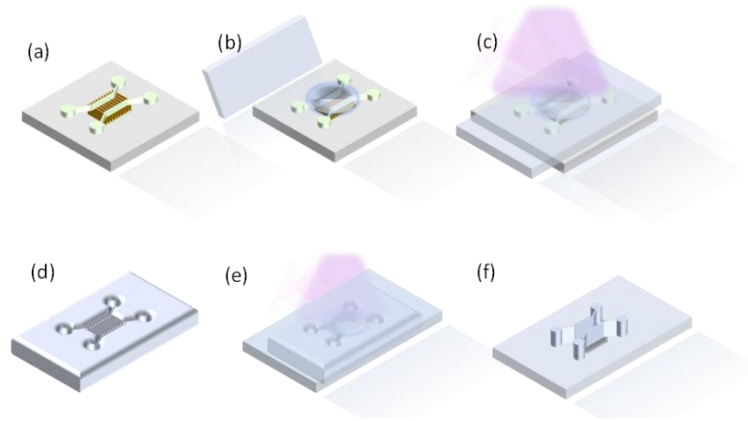


Figure 3-17 Schematic illustration on Ormostamp fabrication procedure. (a) Prepare a master mold; (b) prepare clean glass slide coated with adhesion promotor, apply Ormostamp on master mold; (c) UV cure Ormostamp; (d)-(f) demold Ormostamps from master molds and repeat the process to get an Ormostamp with the same orientation as master molds for nanoimprinting.

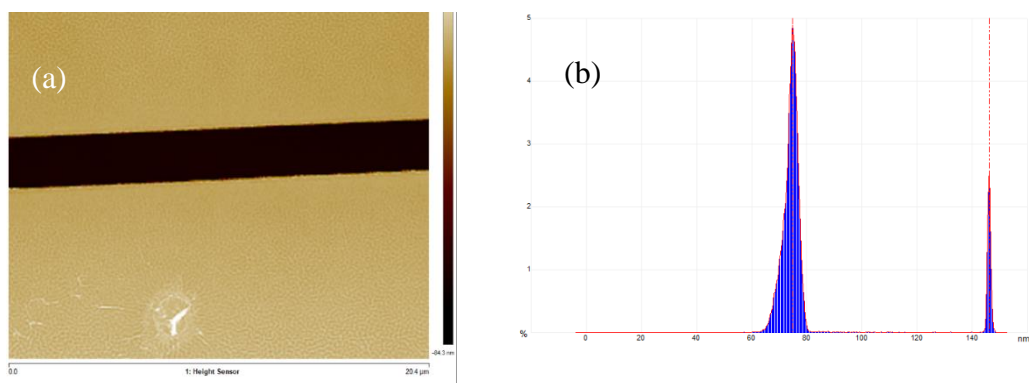


Figure 3-18 (a) AFM images of a microsize mark of PMMA master mold. (b) Peak-to-peak distance on histogram showing the thickness of PMMA is around 71 nm.

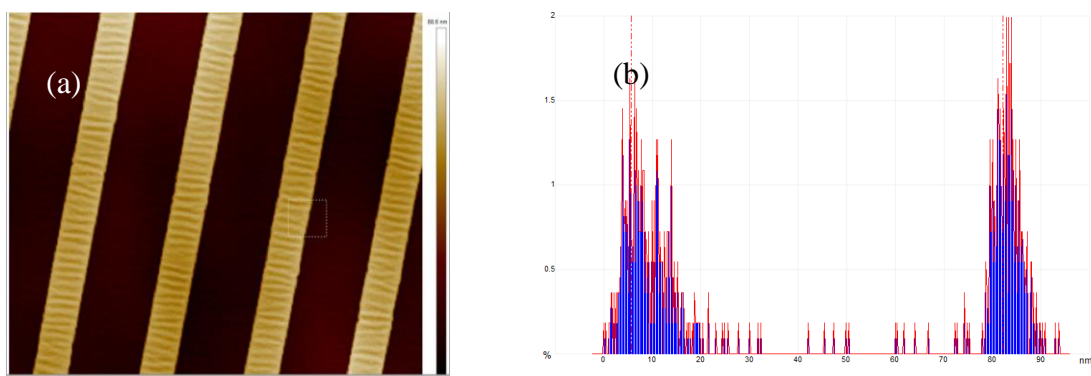


Figure 3-19 (a) AFM image of Ormostamp casted from PMMA nanochannel master on silicon; (b) height profile histogram showing the height of nanochannel walls around 76.5 nm.

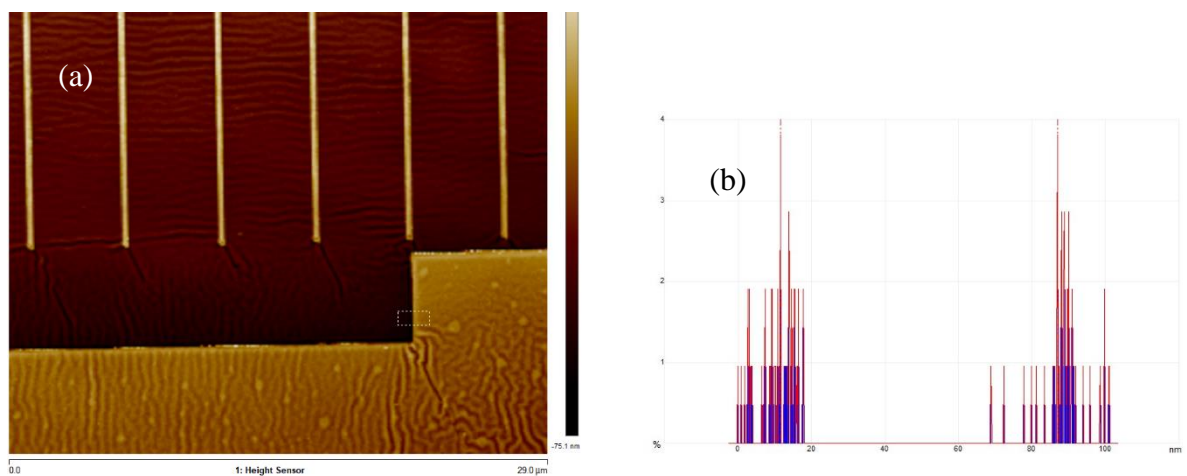


Figure 3-20 AFM height profile characterization of Ormostamp, casted from the PMMA master mold as shown in figure 3-8. (a) Height profile of the Ormostamp containing nanosize ridges; (b) peak-to-peak distance in histogram showing ridges thickness around 75 nm.

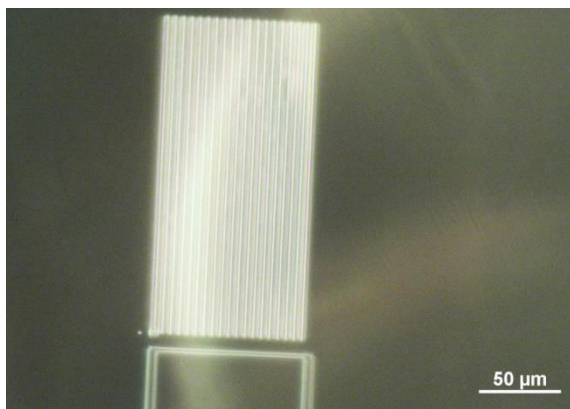


Figure 3-21 Optical microscopy image of nanolines on Ormostamp.

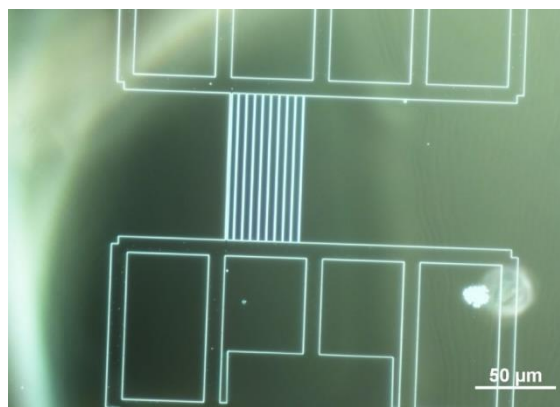


Figure 3-22 Optical microscopy image of microlines and nanolines on Ormostamp.

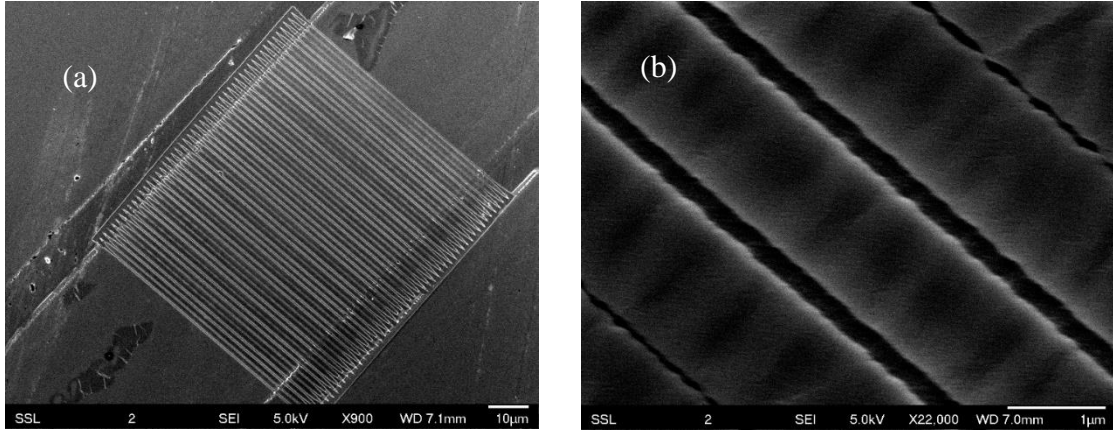


Figure 3-23 SEM of Ormostamp casted from HSQ master resist mold with dimension 132×238 nm. (a) Nanolines connected with microlines. (b) Nanolines.

3.4 Chip replication

3.4.1 PMMA nanoimprinting

Nanoimprinting makes use of rapid change of viscosity and modulus of a polymer around its glass transition temperature. Polymer is at hard elastic state when it is at a temperature below glass transition temperature, T_g . It becomes viscoelastic when the temperature is above T_g but below melting temperature T_m . Heated to a temperature above T_m the polymer become viscous [6]. Nanoimprinting was firstly performed by Chou et al on 55 nm thick PMMA spun on Si substrate with a silicon dioxide mold [91]. PMMA is suitable to be the substrate of imprinting for its ideal release properties, which does not adhere to silicon-based molds. It shrinks less than 0.5% under large changes in temperature and pressure [112], thus owns high fidelity to feature dimensions of molds. 25 nm wide and 100 nm deep features are

formed on PMMA and nanoimprinting is proved to be capable of achieving nano size high aspect ratio structures for fast and large area patterning on polymers.

Here we follow a protocol based on nanoimprinting lithography on thin PMMA films of 175 – 500 μm thickness. To facilitate PMMA LOC devices, the Ormostamp mold is used to imprint on a 175 μm thick PMMA film (PLEXIGLAS[®], 120 °C, 20 bars) for 10 mins, the nanoimprinter used is custom build in our lab. In another 500 μm thick PMMA film (PLEXIGLAS[®]) four 1mm sized holes were drill at specified position, serving as loading reservoirs. PMMA flows into the space in between the protrusions on the stamp. After the chamber is cooled below 70 °C, the pressing pressure is released, and the substrate can be demolded. After Many imprinting attempts showing the imprinting can be done at different temperature and pressure settings. However, higher temperatures (above 130 °C) should not be applied with high imprinting pressure (above 10 bars) to avoid nanostructures deformation. Severe deformation can also be caused by undesired particles and contaminations in between fluidic substrate and molds, which causes warping, substrate bending and undesired air gaps in between substrate and cover plates after bonding. Both those two PMMA films were plasma treated to make them hydrophilic (Harrick, Ossining, NY, 20 W, 300 mTorr, 30 s) and facilitate the bonding process [113].

A kapton film (Kapton[®] HN from DuPont) is cut and placed in imprinting chamber. The procedure should be carried out in a cleanroom as particles beneath imprinting mold may cause breakage when high pressure is applied on the mold. PMMA sheets should be cleaned with IPA. PMMA sheet can be immersed in IPA and cleaned

with sonication. The PMMA piece should be smaller than the Ormostamp mold to prevent breakage and bulging during imprinting process. A kapton film is placed on top for uniform distribution of pressure.

The buffer loading for the untreated PMMA nanochannel is extremely difficult because of the hydrophobicity of the PMMA surface. Plasma treatment can change the PMMA surface hydrophobicity for around 4 hours. To achieve a longer hydrophilic effect, a thin layer of P100d (2000 rpm, 20s, Jonsman Innovation ApS) was spin coated on the imprinted channel before the bonding process. This renders the PMMA surface hydrophilic for 3 days. Figure 3-24 is a SEM image of the nanochannels imprinted on a 175 μm thick PMMA (PLEXIGLAS®).

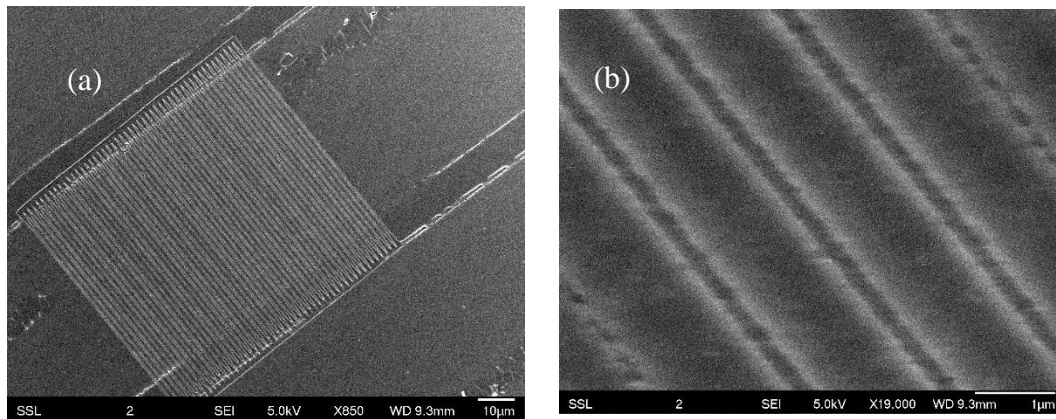


Figure 3-24 (a) SEM image of imprinted nanochannels imprinted using an Ormostamp which is casted from a HSQ resist mold. (b) SEM image with larger magnification. Dimension of the nanochannels is 132 nm \times 210 nm.

Characterization was done on 200 μm thick PMMA sheet (PLEXIGLAS®) with Ormostamp containing nano size ridges patterns. Imprinting tests were conducted in the same chamber. A hotplate was heated to 165 $^{\circ}\text{C}$ and the chamber with PMMA

sheet was placed on the hotplate till the chamber was heated to 120 °C. Apply 20 bars pressure to the chamber and start timing for imprinting during which the chamber temperatures were kept 120 ± 2 °C. Three pieces of PMMA were imprinted for 1, 5, and 10 minutes respectively followed by comparison on imprinted feature dimensions. Nanolines were all transferred to PMMA. Figure 3-25 shows a temperature curve of imprinting chamber where the imprinting temperature 120 °C and 20 bars pressure was hold for 1 minute, after which the chamber was removed from heating plate and cooled down to 70 °C. The hard stamp is released from the polymer substrate at the temperature which the thermal stress induced by cooling is small and the polymer substrate has low distortion probability. It is reported to be 70°C for PMMA [114]. The 20 bars pressure was removed before opening the chamber. The whole imprinting process lasted for less than 30 minutes including heating and cooling, which can be further reduced if heating and cooling equipment is improved. Figure 3-26 and figure 3-27 display the imprinted nanochannels and channel depths measured using AFM tapping mode (Bruker Dimension Icon SPM). A height profile (figure 3-28) from a line scan in AFM showing the surface height differences are within 8 nm. Depth of the imprinted channels are characterized in the height profile histogram by analyzing height profiles at the edge of channel walls and taking the distance between two peaks in the histogram as the channel depth. The depths for PMMA imprinted for 1, 5 and 10 mins are 75.8 nm, 75.5 nm and 73.4 nm respectively (figure 3-29). The differences between the depths are within the surface roughness and measurement error tolerance. AFM is used to measure the height of the channels. The widths of

the channels are not reliably captured using AFM due to tip rounding. No difference in widths of the channels are observed among the three imprinted samples. Thus, imprinting on PMMA can be done in a short time if sufficient high temperature and pressures are applied, and it makes fast and high throughput fabrication possible.

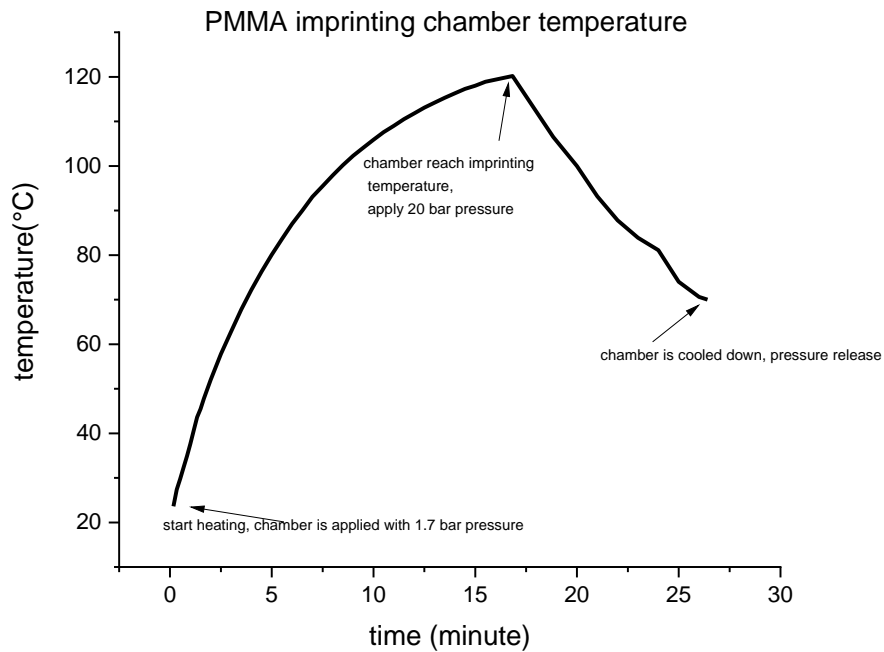


Figure 3-25 Imprinting chamber heating and cooling curve when imprinting is conducted, showing the chamber is held at imprinting 120 °C and 20 bars for 1 minute for imprinting and cooled down.



Figure 3-26 Scanning probe microscopy images on three PMMA pieces imprinted with nanochannel features for (a)1, (b)5 and (c) 10 mins respectively.

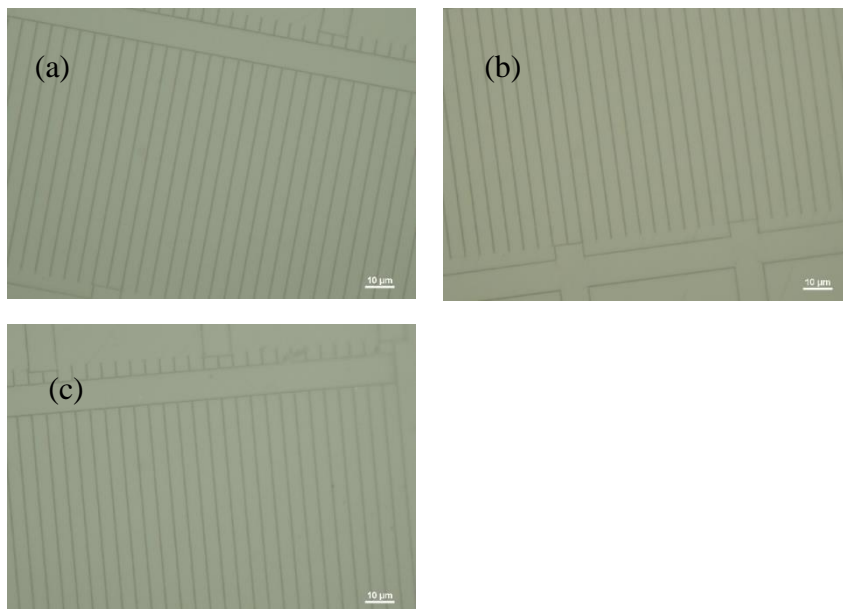


Figure 3-27 Optical microscopy images of the three PMMA pieces imprinted with nanochannel features for (a)1,(b)5 and (c)10 mins respectively.

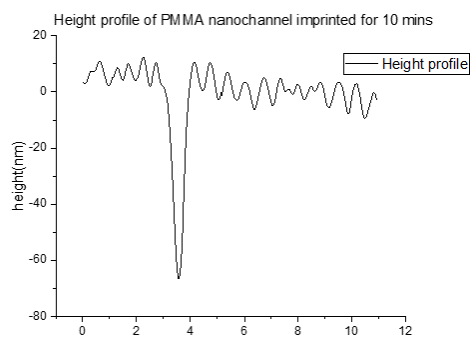
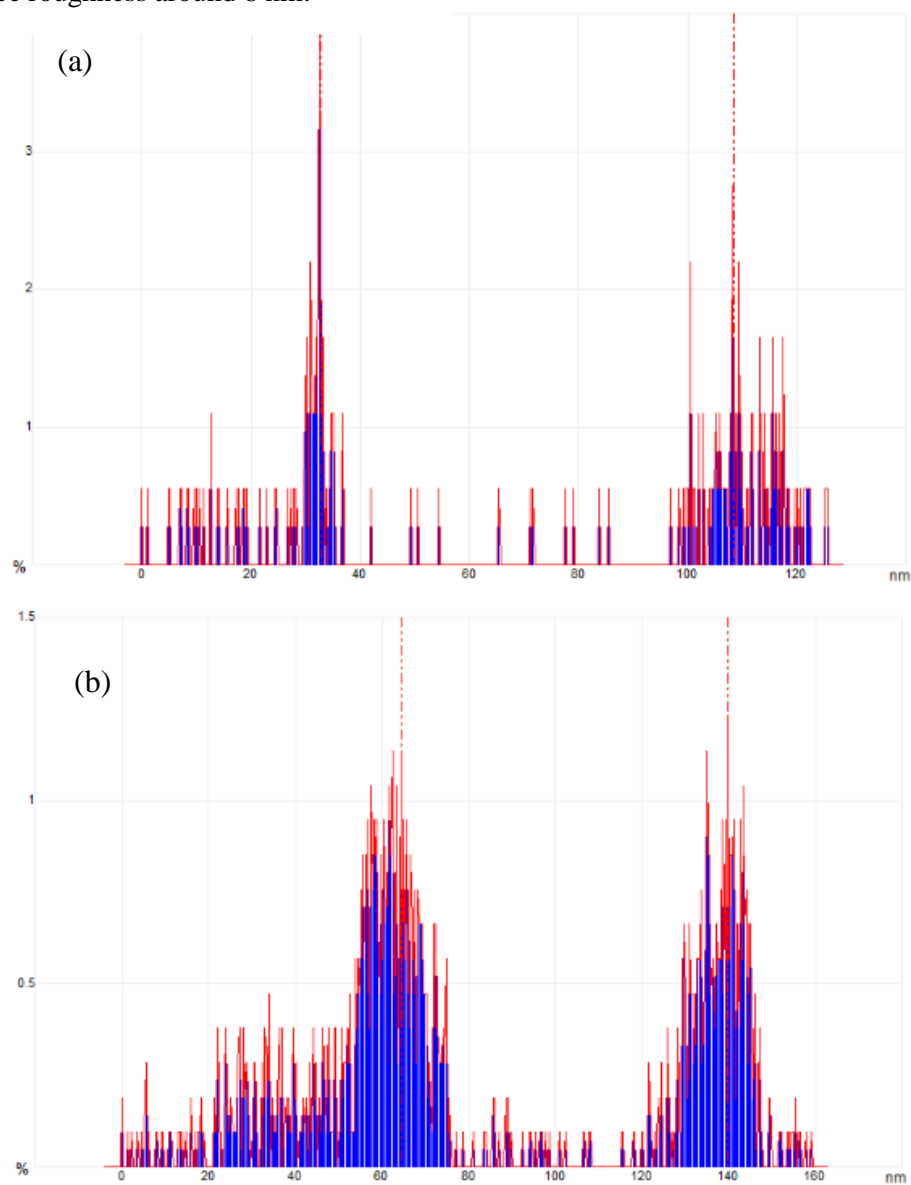


Figure 3-28 A height profile along a line scan from surface probe microscopy on PMMA imprinted for 10 mins, showing a surface roughness around 8 nm.



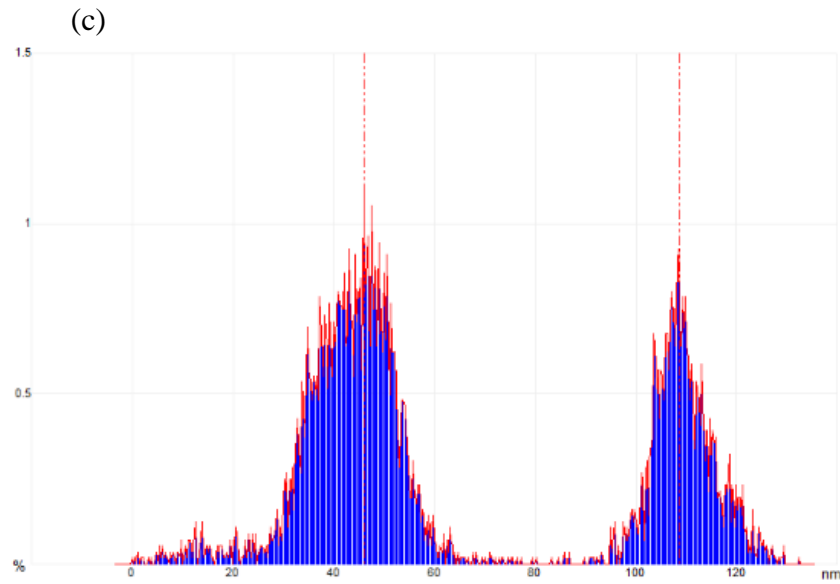


Figure 3-29 AFM images on imprinted PMMA channels, displaying percentages of height profiles (Y axis) over the height information in nm (X axis). Distances between two peaks stand for height difference on PMMA top surface and bottom surface of dented features on the pieces imprinted for (a) 1, (b) 5 and (c) 10 mins, showing channel depths 75.8 nm, 75.5 nm and 73.4 nm respectively. The widths of channels are not captured reliably due to tip rounding.

3.4.2 PDMS and X-PDMS casting

PDMS is used as nanofluidic chip material in biological experiments for the advantages on biologically inert and non-toxic properties, optically transparent which is essential for fluorescence detections. Moreover, there is no etching needed in PDMS chips fabrication process compared to quartz chip fabrication. Nickel molds can be applied to avoid damages to resist layers during casting [41]. A PDMS chips can be fabricated as the following steps. DLC can be coated on Ormostamps before PDMS casting. Mix PDMS elastomer (SylgardTM 184, Dow Corning Co.) and curing agent in 10:1 ratio in weight. Pour the mixture onto an Ormostamp and degas till no bubbles observed on the mixture. Bake the PDMS mixture at 65 °C

oven for 4 hours. Release the mold from the PDMS, punch holes as fluid inlets for the channels. Bond the PDMS with a clean glass slide after plasma treatment (Harrick, Ossining, NY) at 300 mTorr, 80 W for 30 seconds.

Among S-, H- and X- types PDMS, X-PDMS showing the highest rigidity [108][107]. Ormostamp molds can be used for PDMS and X-PDMS casting. A 2 nm DLC carbon layer is coated on the master mold to help in releasing the X-PDMS sample from the Ormostamp mold. The X-PDMS (SCIL Nanoimprint solutions, PHILIPS) is spin coated (2000 rpm, 10s) on the OrmoStamp mold, and cured at 50 °C for 3 mins. After spin coating, the sample is cooled down to room temperature for 6 ~ 10 mins. Another intermediate PDMS layer (SCIL Nanoimprint solutions, PHILIPS) is mixed and spin coated on the OrmoStamp/X-PDMS surface (2000 rpm, 20s), followed by curing at 50 °C for 10 mins and 60 °C for 10 mins. After this, a thicker PDMS (SYLGARD™ 184, Dow Corning) is poured on top of the sample and cured together at 50 °C for 12 h. A plasma treatment (Harrick, Ossining, NY) is applied on the casted PDMS before bonding PDMS with a glass slide.

3.4.3 Sealing nanochannels through bonding

PMMA LOC devices

Thermal bonding is used to make enclosed PMMA micro and nanochannel lab-on-chip devices by sealing the open end of channel pattern without clogging the channel structures. Oxygen plasma treatment prior to thermal bonding enables bonding at a temperature lower than T_g [6][113]. In enclosed PMMA lab on chip devices fabrication, holes are drilled as fluid inlets and outlets before bonding. Plasma treatment (Harrick, Ossining, NY) or P100D coating (2000 rpm, 30 s,

Jonsman Innovation ApS) is applied to PMMA before channel sealing. A 175 μm PMMA sheet imprinted with micro and nanochannel patterns is bonded with a 500 μm PMMA sheet at 1.38 – 1.72 bars, 70 -80 $^{\circ}\text{C}$ for 12-15 mins (figure 3-30).

Timing and energy of plasma treatment should be keep low because plasma oxidation increases surface roughness RMS of PMMA for 10 nm [6]. Bonding temperature and pressure are critical in making PMMA sheet (PLEXIGLAS[®]) bonded while keeping the nano sized structures stand. Higher temperature and lower pressure condition should be applied when the surface is not flat or there are dirt particles on bonding surfaces. During bonding conditions optimization, relative high pressure is coupled with lower temperature. The reason is with higher pressure and temperatures, the bonding strength will be stronger but the dimension of nanochannel will be compromised while for sub 100 nm PMMA nanochannel, lower bonding pressure and temperature should be taken to protect the nanochannel. In a trial of bonding nanosized channel array with dimension around 100 nm wide and 100 nm height, nanochannels collapsed after being in bonding chamber at 89 $^{\circ}\text{C}$, 1.72- 2.06 bars for 15 minutes. Temperature should not be higher than glass transition temperature to prevent the polymer reflow. However, low bonding temperature and pressure may not bond PMMA together. It is found that bonding at 70 $^{\circ}\text{C}$, 1.38 bars for 12 minutes fail to bond PMMA sheets. Thus, the PMMA sheet bonding conditions are found to be 1.38-1.72 bars at 70-80 $^{\circ}\text{C}$.

Other than bonding temperature and pressure, surface flatness and uniformity are essential for getting well bonded chips without air pockets in between two PMMA bulk pieces. Flexible Kapton film is used to ensure a uniform pressure distribution on top of bulk pieces. To improve the surface smoothness of bulk PMMA sheet, bulk PMMA sheet can be pressed onto a silicon wafer at 1.5 bar and 110 °C for 1 hour after drilling of access-holes and prior to thermal bonding [8]. To prevent formation of air bubbles sealed between the bonded surfaces, bulk PMMA sheet can be first heat at 75 °C for 15 minutes to dehydrate before raising the chamber to final pressure and temperature.

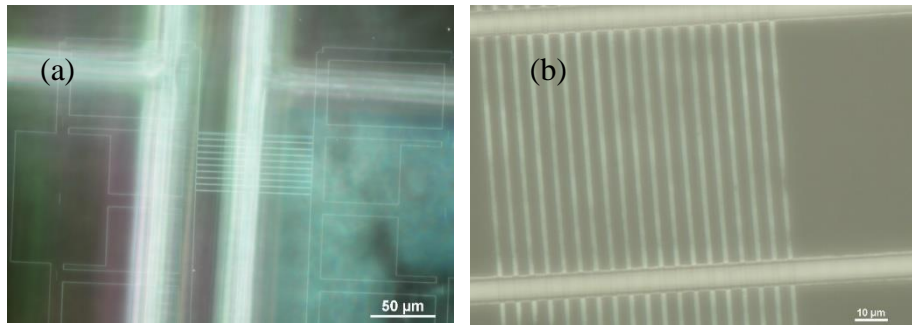


Figure 3-30 Optical microscopy images of enclosed PMMA chips, made by bonding PMMA sheets imprinted with microsize channels and nanosize channels.

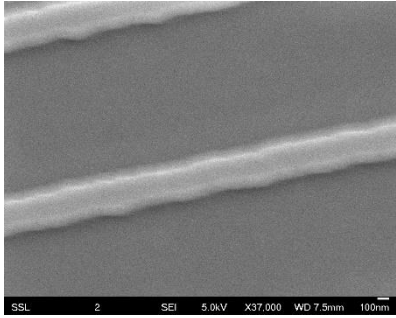
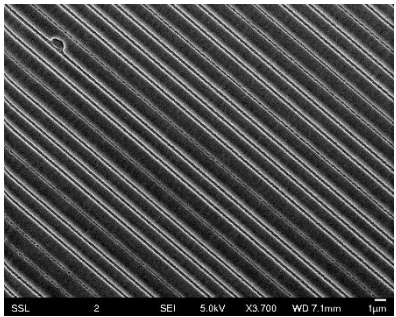
PDMS and X-PDMS LOC devices

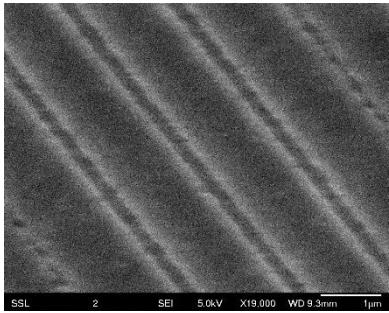
PDMS or X-PDMS can be plasma treated (Harrick, Ossining, NY, 20 s, 300 mTorr, 20 W) and bonded to clean glass slides (100 μm thick). Plasma treatment makes PDMS surface covalent bond exposed thus can be bonded with a glass slide which is treated by plasma as well.

In conclusion, the patterns can be transferred from photoresist master molds to Ormostamp and PMMA substrate with high fidelity in groove and ridge type

structures' dimension. In the examples of resist molds shown in previous sections, PMMA resist molds are patterned by 1.5 MeV H_2^+ beam by moving stage in Y direction and HSQ molds are patterned by scanning the beam in X and Y direction. A table below summaries the feature sizes of nanochannels in resist mold, Ormostamp and imprinted PMMA. The variations are within the measuring errors, thus Ormostamp and imprinting method can transfer the patterns from resist molds, Ormostamp molds to imprinted chips with high fidelity.

Table 3-1. Summary of width of nanochannels on sample master mold, Ormostamp and imprinted nanochannels. The HSQ channels depth is 132 nm. The HSQ master mold is patterned by 1.5 MeV hydrogen molecular beam with beam scanning over X and Y directions.

sample	SEM image	Width of channels
HSQ master mold		231 ± 12 nm
Ormostamp		238 ± 17 nm

<p>Imprinted PMMA channel</p>		<p>$210 \pm 26 \text{ nm}$</p>
-----------------------------------	---	---

Chapter 4 DNA linearization and imaging

4.1 Nanofluidic chips application on DNA sequencing

DNA contains genetic information of cells by specific sequences of base pairs. By knowing the sequences of base pairs and understanding the information like genomic meltdowns helps in understanding the cancers and diagnosis of the diseases. DNA sequencing technologies have been developed for decades while results are compromised by large ensemble averages, noise and systematic errors introduced by polymerase-chain reaction methods and slow analyzing for gel electrophoresis because of loss of length-dependence in electrophoretic mobility [92]. DNA analysis can be done through molecular combing, restriction enzyme sequence-dependent cutting, nano-confinement, linear analysis and optical mapping. Molecules can be linearized by molecular combing through shear stretching by using moving air-liquid meniscus, controlled by electric field and stretch, relax and recoil [115].

Research about DNA has been done in nanochannels devices because the genetic information can be directly readout. Linearizing single-stranded DNA in nanochannels by the self-avoidance interaction is of great interest as any site can be probed by a specific oligonucleotide. Probes can be applied on DNA molecules at higher density in customized sequences. It enables larger scale sequence readout without restriction site motifs [94]. Other than nanochannels, other fluidic devices containing nanoslits, nanopores and zero-mode waveguides are also applied on DNA analysis, providing confining to the molecules [66]. Bottlebrush-coated

single strand DNA can be linearized by nanochannel confinement without recoiling [62]. By integrating nanofluidic channels to lab-on-a-chip devices for DNA investigation, DNA motion can be controlled through confining the molecules in nano size spaces as the thermal motions slow down. With sub hundred nanometer dimension which is at the scale of DNA molecule persistence length, the stretching of DNA molecules are qualitatively inversely proportional to channel dimensions [97]. Large scale genome mapping is achieved by attachment with specific restriction enzyme or by binding gene-targeting probes to the unpaired bases in single stranded DNA. The probes are stained with specific dyes which fluorescence after being excited at certain wavelengths. The application of nanochannels in DNA large scale genome mapping enables assessing genome information in its native state, avoiding cloning and molecular amplification [92]. Enabling fast detections of certain DNA sequences with parallel nanofluidic channel arrays, ease in operation and automatic signal analysis, nanofluidic chips can be widely used in life sciences researches and exhibit potential in cancer diagnosis by indicating genomic meltdowns in a tumor.

4.2 DNA linearization mechanism

The contour length of DNA molecule is the total length of all the base pairs, also the end-to-end length of the molecule. For human genome, the contour length is around 2 m, which equals to $6 \text{ Gbps} \times 0.34 \text{ nm/base pair}$. Persistence length is defined as the length within which the DNA molecule keeps its orientation. It is expressed as the formula: $P = \frac{EI_A}{k_B T}$, E is local Young's modulus of rigidity, I_A

stands for surface moment of inertia of the dsDNA molecule, $k_B T$ is the thermal energy. It can be deduced from the formula that, the persistence length varies upon molecular architecture, absolute temperature and dimension of space. DNA elasticity and thermal stability depend on sequence, for example DNA molecules rich in granine (G) and cytosine (C) are stiffer than adenine (A) and thymine (T) rich molecules. The persistence length of ssDNA and dsDNA are around 0.65 nm and 50 nm respectively [116]. Bottlebrush coating increases the persistence length of dsDNA to 240 nm [117] because the bending rigidity and cross-sectional diameter of the complex are increased.

DNA molecules are a series of blobs which is described in De Gennes blob theory for confined polymers. Chains have finite volume and the blobs are excluded to the others where the molecules are self-avoiding. The persistence length P is defined as the distance in contour over which the DNA molecule ‘forgets’ its orientation [118]. It can be expressed as the scale over which the tangent-tangent correlation function along the molecule contour length decays: $\left\langle \frac{\vec{f}(0,t) \cdot \vec{f}(s,t)}{f(0,t)f(s,t)} \right\rangle = \exp\left(-\frac{s}{P}\right)$, where $\vec{f}(s,t)$ is a tangent vector at a distance s away from position 0. The persistence length is determined by rigidity E , the absolute temperature T and the surface moment of inertia of the DNA molecules I_A : $P = \frac{EI_A}{k_B T}$, and it is regarded as the average of the local sequence variations along the DNA molecule [92]. As the channel width decreases to two times of the persistence length of the molecules (P), DNA are of anisometric blobs structures. When the confinement space decreases to around $2P$ to P , polymers can be characterized as isolated

hairpins. Below persistence length scale, the bending energy increases rapidly while the entropy decreases. The semiflexible polymer can no longer coil as described in the classical Odijk regime [119][120]. The DNA molecules are stretched and trapped in nanochannel because of entropic barrier from narrower channels and shear stretching of molecules in small channels. Inside nanochannels, DNA recoiling would cost more energy than thermal energy, thus allowing the stretched state in statics [121]. Nanofluidics channel speeds up the mapping of restriction-cut DNA segments in minutes compared with conventional pulsed field gel-electrophoresis which usually takes hours to days [122]. Requiring femtogram scale DNA sample, analysis on DNA in a single cell is possible. Molecules with buffer solutions are filled into microchannels through loading reservoirs and facilitated by a combination of diffusion and convection while in nanochannel molecules mainly go through diffusion. Degree of molecule extension not only depend on channel dimension but also chip material surface properties.

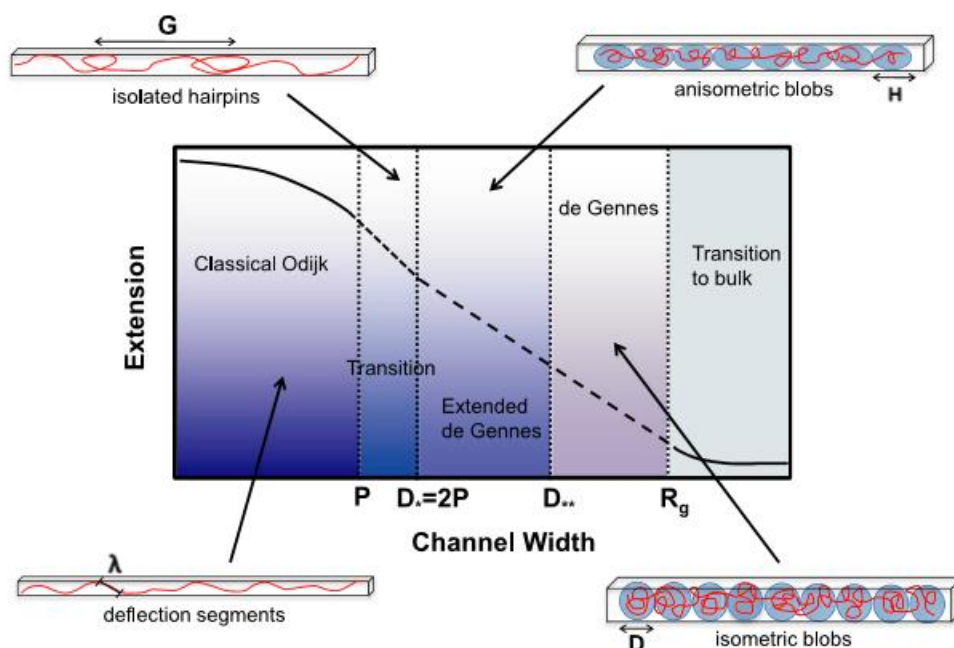


Figure 4-1 Overview of the physical regimes in nanochannel confinements from W Reisner et.al [92]. When the channel dimensions are below the radius-of-gyration R_g , DNA molecules are characterized as isometric blobs in de Gennes regime with geometric average of the channel dimensions D , and the blobs become anisometric below a critical width D^{**} with physical extent H along the channel. At channel dimension P to $2P$, molecules are characterized as isolated hairpins with a global persistence length G . With channel dimensions below P , molecules are extended in nanochannels, characterized by the deflection length λ .

4.3 Experiment method

DNA molecules are stained with YOYO dye half an hour before fluidic experiments. Protein antibody is stained with Alexa dye for one day before imaging.

One drop of stained DNA sample is put on a reservoir which is connected to a microchannel. Wires are immersed into two inlets at each side of nanochannels and a direct voltage of 2 V to 100 V (Keithley, Cleveland, Ohio) is applied to move molecules from one side to the other. The voltage required depends on properties of molecules, in this case, larger voltage 75 V to 100 V is required because DNA together with protein antibody molecules are less charged and heavier, while

moving DNA molecules can be achieved with smaller voltage bias. After introducing molecules into nanochannels, the electric field is powered off and molecules gradually come to equilibrium state in 1 min when they only experience thermal force. Fluorescence images of the DNA molecules are captured by Nikon Eclipse Ti inverted fluorescence microscope with a 100× oil immersion objective. Pictures are taken when laser with different wavelengths is brought to the chip for controlled period of time and exciting different segments of molecules. YOYO is excited by laser with 488 nm wavelength and emits 520 nm wavelength fluorescence. Alexa is excited by laser with 640nm wavelength. After fluorescence imaging, negative bias is applied to move molecules out of the channel and prepare for next round of imaging.

Lambda DNA molecules have been reported to be stretched inside PMMA and PDMS nanochannels with cross section of $120 \times 130 \text{ nm}^2$. DNA fragments are visualized by detecting the fluorescent dye on the molecules after the laser excitation described previously. In fluorescence microscope experiments, fluorescence background from chip materials interferes with signals from fluorescent dye, which limits the detection capability. Aigars Piruska et al reported that 250 μm thick PMMA and 3mm thick PDMS exhibits lower fluorescence intensity compared to PC (polycarbonate) and COC (cyclic olefin copolymer), and are 3 time and 2 times higher than Borofloat [109]. Auto fluorescence from PDMS, PMMA and PC vary at different exciting wavelength and sample thickness.

In the experiment of λ -DNA linearization, molecules are stained with YOYO-1 dye and excited with 488 nm laser. For PMMA chip, the signal-to-noise ratio is 2

to 3 while the ratio is 5 to 7 for X-PDMS chip. The difference in signal-to-noise ratio is not only due to difference in optical properties of these two materials but also the difference in chip carrier. The 500 μm thick PMMA substrates exhibit higher background fluorescence compared to the glass substrates used in X-PDMS chips (100 μm thick). Further improvement on PMMA chips fabrication can be done by utilizing materials with less background fluorescence as substrates or employing thinner PMMA substrates.

Chapter 5 Conclusions

Nanofluidic devices containing hundreds of nanometers features are used for many applications including DNA linearization and large-scale genome mapping. To fulfill the requirement on small feature size, cheap, user-friendly, and high throughput requirements, polymer nanochannel fabrication methods are developed. Combined with proton beam lithography, UV lithography, Ormostamp mold casting and nanoimprinting, PMMA nanochannel chips can be produced in a fast method.

Among the nanopatterning methods, proton beam writing advances in forming high aspect ratio nano ridges or grooves pattern with straight and smooth side walls. The nano ridges or grooves structures are transferred to Ormostamp by UV cure. These Ormostamps can be used in nanoimprinting on PMMA substrate. Lastly, the channels are bonded with PMMA sheet to form enclosed chips by thermal bonding method. The PMMA imprinting can be completed within 30 minutes including heating and cooling procedures. Compared with another widely used polymer chip

material PDMS, PMMA advances in shorter production cycle time by using nanoimprinting methods with optimized heating temperature and bonding pressures while for PDMS casting, long curing time slows the fabrication procedures. Dimensions of the channels and ridges structures formed in the fabrication process are compared and such methods is proven to be able to transfer nanopatterns with high fidelity.

For application on DNA linearization and fluorescence label detection, polymer PMMA and PDMS are chosen as the chip material for the biocompatibility and relative low background fluorescence. PMMA and PDMS surface hydrophilicity can be enhanced by plasma treatment or hydrophilic coating. Other than nanochannels, microchannels and fluid reservoirs structures are essential in a fluidic chip for introducing samples into the interested region. To avoid roof collapse and lateral collapse of channel structure made of soft elastomers, the aspect ratio of the patterns should be controlled. With further improvements on fabrication techniques and reduction of background fluorescence, PMMA nanofluidic chips have great potential in applying for disease diagnostics with developments on mass production, easy operation and highly efficient detections.

Bibliography

- [1] D. J. Tritton and D. J. Tritton, "Low and High Reynolds Numbers," in *Physical Fluid Dynamics*, Springer Netherlands, 1977, pp. 81–87.
- [2] Y. Javadzadeh and S. Hamedeyaz, "Microfluidics and Nanofluidics: Science, Fabrication Microfluidics and Nanofluidics: Science, Fabrication Technology (From Cleanrooms to 3D Printing) and Technology (From Cleanrooms to 3D Printing) and Their Application to Chemical Analysis by Battery- Th," *Trends Helicobacter pylori Infect.*, vol. i, no. tourism, p. 13, 2014.
- [3] J. Fu, P. Mao, and J. Han, "Nanofilter array chip for fast gel-free biomolecule separation," *Appl. Phys. Lett.*, vol. 87, no. 26, pp. 1–3, Dec. 2005.
- [4] T. Yasui *et al.*, "DNA separation in nanowall array chips," *Anal. Chem.*, vol. 83, no. 17, pp. 6635–6640, Sep. 2011.
- [5] P. Abgrall and N. T. Nguyen, "Nanofluidic devices and their applications," *Anal. Chem.*, vol. 80, no. 7, pp. 2326–2341, 2008.
- [6] R. Chantiwas *et al.*, "Flexible fabrication and applications of polymer nanochannels and nanoslits," *Chem. Soc. Rev.*, vol. 40, no. 7, pp. 3677–3702, 2011.
- [7] W. C. Tian and E. Finehout, *Microfluidics for biological applications*. Springer US, 2009.
- [8] W. Liping and A. T. Submitted, "Fabrication of Micro- and Nano- Fluidic Lab-on-a-Chip Devices Utilizing Proton Beam Writing Technique," 2008.
- [9] D. Figeys and D. Pinto, "Lab-on-a-chip: A revolution in biological and medical sciences," *Analytical Chemistry*, vol. 72, no. 9. American Chemical Society, 01-May-2000.
- [10] F. Persson and J. O. Tegenfeldt, "DNA in nanochannels - Directly visualizing genomic information," *Chem. Soc. Rev.*, vol. 39, no. 3, pp. 985–999, 2010.
- [11] I. Yadav, W. Rosencrans, R. Basak, J. A. van Kan, and J. R. C. van der Maarel, "Intramolecular dynamics of dsDNA confined to a quasi-one-dimensional nanochannel," *Phys. Rev. Res.*, vol. 2, no. 1, 2020.
- [12] M. R. Powell *et al.*, "Nanoprecipitation-assisted ion current oscillations," *Nat. Nanotechnol.*, vol. 3, no. 1, pp. 51–57, Jan. 2008.
- [13] H. Yin, G. McPhee, and P. Dobson, "Micro/nanoengineering and AFM for Cellular Sensing," in *Atomic Force Microscopy in Process Engineering*, Elsevier Ltd, 2009, pp. 195–224.
- [14] C. Y and P. A, "Nanofabrication: Conventional and Nonconventional Methods," *Electrophoresis*, vol. 22, no. 2, 2001.
- [15] A. A. Tseng, "Recent developments in nanofabrication using focused ion beams," *Small*, vol. 1, no. 10. Small, pp. 924–939, Sep-2005.
- [16] P. Rodgers, "What diffraction limit?," *Nat. Nanotechnol.*, pp. 1–1, Apr. 2009.
- [17] M. F. Ashby, P. J. Ferreira, and D. L. Schodek, "Nanomaterials: Synthesis and

- Characterization,” in *Nanomaterials, Nanotechnologies and Design*, Elsevier, 2009, pp. 257–290.
- [18] J. M. Perry, K. Zhou, Z. D. Harms, and S. C. Jacobson, “Ion transport in nanofluidic funnels,” *ACS Nano*, vol. 4, no. 7, pp. 3897–3902, Jul. 2010.
 - [19] S. H. Kim *et al.*, “Simple fabrication of hydrophilic nanochannels using the chemical bonding between activated ultrathin PDMS layer and cover glass by oxygen plasma,” *Lab Chip*, vol. 11, no. 2, pp. 348–353, Jan. 2011.
 - [20] A. A. Tseng, “TOPICAL REVIEW Recent developments in micromilling using focused ion beam technology,” *Inst. Phys. Publ. J. MICROMECHANICS MICROENGINEERING J. Micromech. Microeng.*, vol. 14, pp. 15–34, 2004.
 - [21] P. Chen, J. Gu, E. Brandin, Y. R. Kim, Q. Wang, and D. Branton, “Probing single DNA molecule transport using fabricated nanopores,” *Nano Lett.*, vol. 4, no. 11, pp. 2293–2298, Nov. 2004.
 - [22] L. D. Menard and J. M. Ramsey, “Fabrication of sub-5 nm nanochannels in insulating substrates using focused ion beam milling,” *Nano Lett.*, vol. 11, no. 2, pp. 512–517, 2011.
 - [23] T. Maleki, S. Mohammadi, and B. Ziaie, “A nanofluidic channel with embedded transverse nanoelectrodes,” *Nanotechnology*, vol. 20, no. 10, p. 105302, Mar. 2009.
 - [24] L. J. Guo, “Nanoimprint lithography: Methods and material requirements,” *Adv. Mater.*, vol. 19, no. 4, pp. 495–513, Feb. 2007.
 - [25] S. Kim, G. H. Kim, H. Woo, T. An, and G. Lim, “Fabrication of a Novel Nanofluidic Device Featuring ZnO Nanochannels,” *ACS Omega*, vol. 5, no. 7, pp. 3144–3150, Feb. 2020.
 - [26] D. Xia, Z. Ku, S. C. Lee, and S. R. J. Brueck, “Nanostructures and Functional Materials Fabricated by Interferometric Lithography,” *Adv. Mater.*, vol. 23, no. 2, pp. 147–179, Jan. 2011.
 - [27] G. Zhang and D. Wang, “Colloidal Lithography-The Art of Nanochemical Patterning FOCUS REVIEWS,” vol. 4, pp. 236–245, 2009.
 - [28] D. Mijatovic, J. C. T. Eijkel, and A. Van Den Berg, “Technologies for nanofluidic systems: Top-down vs. bottom-up - A review,” *Lab on a Chip*, vol. 5, no. 5. Royal Society of Chemistry, pp. 492–500, 26-Apr-2005.
 - [29] J. Haneveld, H. V. Jansen, J. W. Berenschot, N. R. Tas, and M. C. Elwenspoek, “Wet anisotropic etching for fluidic 1D nanochannels.” *MicroMechanics Europe*, pp. 47–50, 06-Oct-2002.
 - [30] W. P. Shin, C. Y. Hui, and N. C. Tien, “Collapse of microchannels during anodic bonding: Theory and experiments,” *J. Appl. Phys.*, vol. 95, no. 5, pp. 2800–2808, Mar. 2004.
 - [31] C. Duan, W. Wang, and Q. Xie, *Review article: Fabrication of nanofluidic devices*, vol. 7, no. 2. 2013.
 - [32] D. Stein, Z. Deurvorst, F. H. J. Van Der Heyden, W. J. A. Koopmans, A. Gabel, and C. Dekker, “Electrokinetic concentration of DNA polymers in nanofluidic channels,” *Nano Lett.*, vol. 10, no. 3, pp. 765–772, Mar. 2010.

- [33] P. Mao and J. Han, "Fabrication and characterization of 20 nm planar nanofluidic channels by glass-glass and glass-silicon bonding," *Lab Chip*, vol. 5, no. 8, pp. 837–844, Jul. 2005.
- [34] L. Ji, J.-K. Kim, Q. Ji, K.-N. Leung, Y. Chen, and R. A. Gough, "Conformal metal thin-film coatings in high-aspect-ratio trenches using a self-sputtered rf-driven plasma source," *J. Vac. Sci. Technol. B Microelectron. Nanom. Struct.*, vol. 25, no. 4, p. 1227, Jun. 2007.
- [35] P. Mao and J. Han, "Massively-parallel ultra-high-aspect-ratio nanochannels as mesoporous membranes," *Lab Chip*, vol. 9, no. 4, pp. 586–591, Feb. 2009.
- [36] J. C. Love, K. E. Paul, and G. M. Whitesides, "Fabrication of Nanometer-Scale Features by Controlled Isotropic Wet Chemical Etching," *Adv. Mater.*, vol. 13, no. 8, pp. 604–607, Apr. 2001.
- [37] K. Tybrandt, R. Forchheimer, and M. Berggren, "Logic gates based on ion transistors," *Nat. Commun.*, vol. 3, no. 1, pp. 1–6, May 2012.
- [38] S. P. Adiga, C. Jin, L. A. Curtiss, N. A. Monteiro-Riviere, and R. J. Narayan, "Nanoporous membranes for medical and biological applications."
- [39] F. Li, L. Zhang, and R. M. Metzger, "On the Growth of Highly Ordered Pores in Anodized Aluminum Oxide," *Chem. Mater.*, vol. 10, no. 9, pp. 2470–2480, 1998.
- [40] K. Ansari, J. A. Van Kan, A. A. Bettiol, and F. Watt, "Stamps for nanoimprint lithography fabricated by proton beam writing and nickel electroplating," *J. Micromechanics Microengineering*, vol. 16, no. 10, pp. 1967–1974, 2006.
- [41] F. Liu, K. B. Tan, P. Malar, S. K. Bikkarolla, and J. A. Van Kan, "Fabrication of nickel molds using proton beam writing for micro/nano fluidic devices," *Microelectron. Eng.*, vol. 102, pp. 36–39, 2013.
- [42] J. Taniguchi *et al.*, "Diamond mold for nanoimprint lithography," in *Digest of Papers - 2000 International Microprocesses and Nanotechnology Conference, MNC 2000*, 2000, pp. 190–191.
- [43] J. Taniguchi *et al.*, "Preparation of diamond mold using electron beam lithography for application to nanoimprint lithography," *Japanese J. Appl. Physics, Part 1 Regul. Pap. Short Notes Rev. Pap.*, vol. 39, no. 12 B, pp. 7070–7074, 2000.
- [44] G. A. Glass *et al.*, "High energy focused ion beam lithography using P-beam writing," *Nucl. Instruments Methods Phys. Res. Sect. B Beam Interact. with Mater. Atoms*, vol. 241, no. 1–4, pp. 397–401, Dec. 2005.
- [45] T. C. Sum, A. A. Bettiol, H. L. Seng, I. Rajta, J. A. Van Kan, and F. Watt, "Proton beam writing of passive waveguides in PMMA," *Nucl. Instruments Methods Phys. Res. Sect. B Beam Interact. with Mater. Atoms*, vol. 210, pp. 266–271, 2003.
- [46] F. Picollo *et al.*, "Fabrication of monolithic microfluidic channels in diamond with ion beam lithography," *Nucl. Instruments Methods Phys. Res. Sect. B Beam Interact. with Mater. Atoms*, 2017.
- [47] J. P. Biersack and L. G. Haggmark, "A Monte Carlo computer program for the transport of energetic ions in amorphous targets," *Nucl. Instruments Methods*, vol. 174, no. 1–2, pp. 257–269, Aug. 1980.
- [48] J. A. Van Kan, A. A. Bettiol, and F. Watt, "Proton beam writing of three-

- dimensional nanostructures in hydrogen silsesquioxane,” *Nano Lett.*, vol. 6, no. 3, pp. 579–582, 2006.
- [49] H. D. Liang *et al.*, “High aspect ratio channels in glass and porous silicon,” *Nucl. Instruments Methods Phys. Res. Sect. B Beam Interact. with Mater. Atoms*, vol. 394, pp. 1–5, 2017.
 - [50] S. Punniyakoti *et al.*, “Hydrogen Silsesquioxane-Based Nanofluidics,” *Adv. Mater. Interfaces*, vol. 4, no. 7, 2017.
 - [51] B. Rout, M. Kamal, A. D. Dymnikov, D. P. Zachry, and G. A. Glass, “Fabrication of micro-structured tunnels in PMMA using P-beam writing,” *Nucl. Instruments Methods Phys. Res. Sect. B Beam Interact. with Mater. Atoms*, vol. 260, no. 1, pp. 366–371, Jul. 2007.
 - [52] J. A. Van Kan, P. Malar, and A. Baysic De Vera, “The second generation Singapore high resolution proton beam writing facility,” *Rev. Sci. Instrum.*, vol. 83, no. 2, 2012.
 - [53] J. A. Van Kan, P. Malar, and Y. H. Wang, “Resist materials for proton beam writing: A review,” *Appl. Surf. Sci.*, vol. 310, pp. 100–111, 2014.
 - [54] E. Lee and J. W. Hahn, “The effect of photoresist contrast on the exposure profiles obtained with evanescent fields of nanoapertures,” *J. Appl. Phys.*, vol. 103, no. 8, 2008.
 - [55] Y. H. Wang, P. Malar, and J. A. van Kan, “Resist evaluation for proton beam writing, Ni mold fabrication and nano-replication,” *Microsyst. Technol.*, vol. 20, no. 10–11, pp. 2079–2088, Oct. 2014.
 - [56] J. A. Van Kan, A. A. Bettiol, and F. Watt, “Three-dimensional nanolithography using proton beam writing,” *Appl. Phys. Lett.*, vol. 83, no. 8, pp. 1629–1631, 2003.
 - [57] S. Bolhuis, J. A. van Kan, and F. Watt, “Enhancement of proton beam writing in PMMA through optimization of the development procedure,” *Nucl. Instruments Methods Phys. Res. Sect. B Beam Interact. with Mater. Atoms*, vol. 267, no. 12–13, pp. 2302–2305, 2009.
 - [58] F. Menzel, D. Spemann, S. Petriconi, J. Lenzner, and T. Butz, “Proton beam writing of microstructures at the ion nanoprobe LIPSION,” *Nucl. Instruments Methods Phys. Res. Sect. B Beam Interact. with Mater. Atoms*, vol. 250, no. 1-2 SPEC. ISS., pp. 66–70, 2006.
 - [59] C. L. Frye, W. T. Collins, A. J. Barry, W. H. Daudt, J. J. Domicone, and J. W. Gilkey, “The Oligomeric Silsesquioxanes, (HSiO₂)_n,” 1955.
 - [60] F. C. M. J. M. Van Delft, “Delay-time and aging effects on contrast and sensitivity of hydrogen silsesquioxane,” *J. Vac. Sci. Technol. B Microelectron. Nanom. Struct.*, vol. 20, no. 6, pp. 2932–2936, 2002.
 - [61] S. Pennathur and J. G. Santiago, “Electrokinetic transport in nanochannels. 2. Experiments,” *Anal. Chem.*, vol. 77, no. 21, pp. 6782–6789, Nov. 2005.
 - [62] R. Basak *et al.*, “Linearization and Labeling of Single-Stranded DNA for Optical Sequence Analysis,” *J. Phys. Chem. Lett.*, pp. 316–321, 2019.
 - [63] J. J. Jones, J. R. C. Van Der Maarel, and P. S. Doyle, “Macromolecular Crowding,” *SpringerReference*, pp. 5047–5053, 2011.

- [64] C. Zhang, K. Jiang, F. Liu, P. S. Doyle, J. A. Van Kan, and J. R. C. Van Der Maarel, "A nanofluidic device for single molecule studies with in situ control of environmental solution conditions," *Lab Chip*, vol. 13, no. 14, pp. 2821–2826, 2013.
- [65] J. R. C. van der Maarel, C. Zhang, and J. A. van Kan, "A Nanochannel Platform for Single DNA Studies: From Crowding, Protein DNA Interaction, to Sequencing of Genomic Information," *Isr. J. Chem.*, vol. 54, no. 11–12, pp. 1573–1588, 2014.
- [66] S. L. Levy and H. G. Craighead, "DNA manipulation, sorting, and mapping in nanofluidic systems," *Chem. Soc. Rev.*, vol. 39, no. 3, pp. 1133–1152, 2010.
- [67] F. Watt *et al.*, "The National University of Singapore high energy ion nano-probe facility: Performance tests," *Nucl. Instruments Methods Phys. Res. Sect. B Beam Interact. with Mater. Atoms*, vol. 210, pp. 14–20, Sep. 2003.
- [68] F. Watt *et al.*, "The National University of Singapore nuclear microscope facility," *Nucl. Inst. Methods Phys. Res. B*, vol. 85, no. 1–4, pp. 708–715, 1994.
- [69] D. J. W. Mous, R. G. Haitzma, T. Butz, R.-H. Flaggmeyer, D. Lehmann, and J. Vogt, "The novel ultrastable HVEE 3.5 MV Singletron™ accelerator for nanoprobe applications," *Nucl. Instruments Methods Phys. Res. Sect. B Beam Interact. with Mater. Atoms*, vol. 130, no. 1–4, pp. 31–36, 1997.
- [70] S. Qureshi, "NANOFABRICATION USING OPTIMIZED PROTON BEAM WRITING AND MASKED ION LITHOGRAPHY," 2018.
- [71] J. A. Van Kan, P. Malar, A. B. De Vera, X. Chen, A. A. Bettiol, and F. Watt, "Proton beam writing nanoprobe facility design and first test results," *Nucl. Instruments Methods Phys. Res. Sect. A Accel. Spectrometers, Detect. Assoc. Equip.*, vol. 645, no. 1, pp. 113–115, 2011.
- [72] J. A. van Kan, P. Malar, and A. Baysic de Vera, "The second generation Singapore high resolution proton beam writing facility," *Rev. Sci. Instrum.*, vol. 83, no. 2, p. 02B902, Feb. 2012.
- [73] Y. Yao and J. A. Van Kan, "Automatic beam focusing in the 2nd generation PBW line at sub-10 nm line resolution," *Nucl. Instruments Methods Phys. Res. Sect. B Beam Interact. with Mater. Atoms*, vol. 348, pp. 203–208, 2015.
- [74] F. Watt, I. Rajta, J. A. Van Kan, A. A. Bettiol, and T. Osipowicz, "Proton beam micromachined resolution standards for nuclear microprobes," *Nucl. Instruments Methods Phys. Res. Sect. B Beam Interact. with Mater. Atoms*, vol. 190, no. 1–4, pp. 306–311, 2002.
- [75] Y. Yao, M. W. Van Mourik, P. Santhana Raman, and J. A. Van Kan, "Improved beam spot measurements in the 2nd generation proton beam writing system," *Nucl. Instruments Methods Phys. Res. Sect. B Beam Interact. with Mater. Atoms*, vol. 306, pp. 265–270, 2013.
- [76] S. Qureshi, P. S. Raman, A. Stegmaier, and J. A. van Kan, "Quadrupole lens alignment with improved STIM and secondary electron imaging for Proton Beam Writing," *Nucl. Instruments Methods Phys. Res. Sect. B Beam Interact. with Mater. Atoms*, vol. 404, pp. 74–80, 2017.
- [77] S. Qureshi, W. Jiacheng, and J. A. van Kan, "Automated alignment and focusing system for nuclear microprobes," *Nucl. Instruments Methods Phys. Res. Sect. B Beam Interact. with Mater. Atoms*, vol. 456, no. July 2018, pp. 80–85, 2019.

- [78] C. N. B. Udalagama *et al.*, “An automatic beam focusing system for MeV protons,” *Nucl. Instruments Methods Phys. Res. Sect. B Beam Interact. with Mater. Atoms*, vol. 231, no. 1–4, pp. 389–393, 2005.
- [79] Y. Yao and J. A. Van Kan, “Automatic beam focusing in the 2nd generation PBW line at sub-10 nm line resolution,” *Nucl. Instruments Methods Phys. Res. Sect. B Beam Interact. with Mater. Atoms*, vol. 348, 2015.
- [80] A. A. Bettiol, C. N. B. Udalagama, J. A. Van Kan, and F. Watt, “Ionscan: Scanning and control software for proton beam writing,” *Nucl. Instruments Methods Phys. Res. Sect. B Beam Interact. with Mater. Atoms*, vol. 231, no. 1–4, pp. 400–406, 2005.
- [81] X. Chen and L. Zhang, “Review in manufacturing methods of nanochannels of bio-nanofluidic chips,” *Sensors and Actuators, B: Chemical*, vol. 254. Elsevier B.V., pp. 648–659, 01-Jan-2018.
- [82] J. Wang, Y. Yan, Y. Geng, Y. Gan, and Z. Fang, “Fabrication of polydimethylsiloxane nanofluidic chips under AFM tip-based nanomilling process,” *Nanoscale Res. Lett.*, vol. 14, no. 1, p. 136, Dec. 2019.
- [83] T. H. P. Chang, M. Mankos, K. Y. Lee, and L. P. Muray, “Multiple electron-beam lithography,” *Microelectron. Eng.*, vol. 57–58, pp. 117–135, Sep. 2001.
- [84] J. J. Kochumalayil, A. Meiser, F. Soldera, and W. Possart, “Focused ion beam irradiation-morphological and chemical evolution in PMMA,” *Surf. Interface Anal.*, vol. 41, no. 5, pp. 412–420, May 2009.
- [85] K. Yamasaki, S. Juodkazis, S. Matsuo, and H. Misawa, “Three-dimensional micro-channels in polymers: One-step fabrication,” *Appl. Phys. A Mater. Sci. Process.*, vol. 77, no. 3–4, pp. 371–373, Aug. 2003.
- [86] L. P. Wang, P. G. Shao, J. A. van Kan, A. A. Bettiol, and F. Watt, “Development of elastomeric lab-on-a-chip devices through Proton Beam Writing (PBW) based fabrication strategies,” *Nucl. Instruments Methods Phys. Res. Sect. B Beam Interact. with Mater. Atoms*, vol. 267, no. 12–13, pp. 2312–2316, 2009.
- [87] L. P. Wang *et al.*, “Fabrication of nanofluidic devices utilizing proton beam writing and thermal bonding techniques,” *Nucl. Instruments Methods Phys. Res. Sect. B Beam Interact. with Mater. Atoms*, vol. 260, no. 1, pp. 450–454, Jul. 2007.
- [88] H. Cao *et al.*, “Fabrication of 10 nm enclosed nanofluidic channels,” *Appl. Phys. Lett.*, vol. 81, no. 1, pp. 174–176, 2002.
- [89] J. Fu *et al.*, “Fabrication of microchannels in single crystal diamond for microfluidic systems,” *Microfluid. Nanofluidics*, vol. 22, no. 9, pp. 1–5, 2018.
- [90] K. A. Mahabadi, I. Rodriguez, S. C. Haur, J. A. Van Kan, A. A. Bettiol, and F. Watt, “Fabrication of PMMA micro- and nanofluidic channels by proton beam writing: Electrokinetic and morphological characterization,” *J. Micromechanics Microengineering*, vol. 16, no. 7, pp. 1170–1180, 2006.
- [91] S. Y. Chou, P. R. Krauss, and P. J. Renstrom, “Imprint of sub-25 nm vias and trenches in polymers,” *Appl. Phys. Lett.*, vol. 67, no. 1, p. 3114, 1995.
- [92] W. Reisner, J. N. Pedersen, and R. H. Austin, “DNA confinement in nanochannels: Physics and biological applications,” *Reports Prog. Phys.*, vol. 75, no. 10, 2012.
- [93] H. Lan, “Large-Area Nanoimprint Lithography and Applications,” in

Micro/Nanolithography - A Heuristic Aspect on the Enduring Technology, InTech, 2018.

- [94] R. Basak *et al.*, “Linearization and Labeling of Single-Stranded DNA for Optical Sequence Analysis,” *J. Phys. Chem. Lett.*, pp. 316–321, 2019.
- [95] E. Abad, S. Merino, A. Retolaza, and A. Juarros, “Design and fabrication using nanoimprint lithography of a nanofluidic device for DNA stretching applications,” *Microelectron. Eng.*, vol. 85, no. 5–6, pp. 818–821, 2008.
- [96] L. H. Thamdrup, A. Klukowska, and A. Kristensen, “Stretching DNA in polymer nanochannels fabricated by thermal imprint in PMMA,” *Nanotechnology*, vol. 19, no. 12, 2008.
- [97] L. J. Guo, X. Cheng, and C. F. Chou, “Fabrication of Size-Controllable Nanofluidic Channels by Nanoimprinting and Its Application for DNA Stretching,” *Nano Lett.*, vol. 4, no. 1, pp. 69–73, 2004.
- [98] S. W. Turner, A. M. Perez, A. Lopez, and H. G. Craighead, “Monolithic nanofluid sieving structures for DNA manipulation,” *J. Vac. Sci. Technol. B Microelectron. Nanom. Struct.*, vol. 16, no. 6, pp. 3835–3840, 1998.
- [99] W. Li *et al.*, “Sacrificial polymers for nanofluidic channels in biological applications,” *Nanotechnology*, vol. 14, no. 6, pp. 578–583, Jun. 2003.
- [100] P. E. Shao, A. Van Kan, L. P. Wang, K. Ansari, A. A. Bettiol, and F. Watt, “Fabrication of enclosed nanochannels in poly(methylmethacrylate) using proton beam writing and thermal bonding,” *Appl. Phys. Lett.*, vol. 88, no. 9, pp. 2004–2007, 2006.
- [101] Y. H. Wang, P. Malar, and J. A. van Kan, “Resist evaluation for proton beam writing, Ni mold fabrication and nano-replication,” *Microsyst. Technol.*, vol. 20, no. 10–11, pp. 2079–2088, Oct. 2014.
- [102] F. Liu, Y. Yao, and J. A. Van Kan, “OrmoStamp mold fabrication via PBW for NIL,” *Nucl. Instruments Methods Phys. Res. Sect. B Beam Interact. with Mater. Atoms*, vol. 348, pp. 229–232, 2015.
- [103] I. Fernandez-Cuesta *et al.*, “Fabrication of fluidic devices with 30 nm nanochannels by direct imprinting,” *J. Vac. Sci. Technol. B, Nanotechnol. Microelectron. Mater. Process. Meas. Phenom.*, vol. 29, no. 6, p. 06F801, 2011.
- [104] J. A. Van Kan, I. Rajta, K. Ansari, A. A. Bettiol, and F. Watt, “Nickel and copper electroplating of proton beam micromachined SU-8 resist,” *Microsyst. Technol.*, vol. 8, no. 6, pp. 383–386, 2002.
- [105] D. C. Duffy, J. C. McDonald, O. J. A. Schueller, and G. M. Whitesides, “Rapid prototyping of microfluidic systems in poly(dimethylsiloxane),” *Anal. Chem.*, vol. 70, no. 23, pp. 4974–4984, 1998.
- [106] Z. jun Zhao, J. ho Yang, and S. hu Park, “Step-and-repeat stamping method for the generation of large-area microscale wrinkle patterns,” *J. Mech. Sci. Technol.*, vol. 31, no. 4, pp. 1893–1898, Apr. 2017.
- [107] M. Scharin-Mehlmann *et al.*, “Nano- and micro-patterned S-, H-, and X-PDMS for cell-based applications: Comparison of wettability, roughness, and cell-derived parameters,” *Front. Bioeng. Biotechnol.*, vol. 6, no. MAY, pp. 1–13, 2018.

- [108] M. A. Verschuuren, *Verschuuren - Substrate Conformal Imprint Lithography for Nanophotonics*. .
- [109] A. Piruska *et al.*, “The autofluorescence of plastic materials and chips measured under laser irradiation,” *Lab Chip*, vol. 5, no. 12, pp. 1348–1354, 2005.
- [110] J. Han, S. W. Turner, and H. G. Craighead, “Entropic trapping and escape of long DNA molecules at submicron size constriction,” *Phys. Rev. Lett.*, vol. 83, no. 8, pp. 1688–1691, 1999.
- [111] Micro Resist Technologies, “Processing Guidelines - OrmoStamp,” *Micro Resist Technologies*, 2012. .
- [112] I. I. Rubin, *Injection molding; theory and practice*. New York,: Wiley, 1973.
- [113] P. Abgrall, L. N. Low, and N. T. Nguyen, “Fabrication of planar nanofluidic channels in a thermoplastic by hot-embossing and thermal bonding,” *Lab Chip*, vol. 7, no. 4, pp. 520–522, 2007.
- [114] A. Amirsadeghi, J. J. Lee, and S. Park, “Polymerization shrinkage stress measurement for a UV-curable resist in nanoimprint lithography,” *J. Micromechanics Microengineering*, vol. 21, no. 11, 2011.
- [115] J. T. Mannion, C. H. Reccius, J. D. Cross, and H. G. Craighead, “Conformational analysis of single DNA molecules undergoing entropically induced motion in nanochannels,” *Biophys. J.*, vol. 90, no. 12, pp. 4538–4545, 2006.
- [116] D. B. McIntosh and O. A. Saleh, “Salt species-dependent electrostatic effects on ssDNA elasticity,” *Macromolecules*, vol. 44, no. 7, pp. 2328–2333, Apr. 2011.
- [117] “Amplified stretch of bottlebrush-coated DNA in nanofluidic channels.” [Online]. Available: <https://www.ncbi.nlm.nih.gov/pmc/articles/PMC3814371/>. [Accessed: 10-May-2020].
- [118] “DNA Topology - Andrew D Bates, Anthony Maxwell - Oxford University Press.” [Online]. Available: <https://global.oup.com/academic/product/dna-topology-9780198506553?cc=sg&lang=en&>. [Accessed: 19-Aug-2020].
- [119] E. Straube, “Scaling concepts in polymer physics. Von P. G. DE GENNES. Ithaca/London: Cornell University Press 1980. Geb., £ 23,-, \$ 48.-,” *Acta Polym.*, vol. 32, no. 5, pp. 290–290, May 1981.
- [120] M. Daoud and P. G. De Gennes, “Statistics of macromolecular solutions trapped in small pores,” *J. Phys.*, vol. 38, no. 1, 1977.
- [121] A. Reina, A. B. Subramaniam, A. Laromaine, A. D. T. Samuel, and G. M. Whitesides, “Shifts in the Distribution of Mass Densities Is a Signature of Caloric Restriction in *Caenorhabditis elegans*,” *PLoS One*, vol. 8, no. 7, 2013.
- [122] H. Gutfreund, “Protein-DNA Interactions (Methods in ENZYMOLOGY, Vol. 208),” vol. 313, no. 3, pp. 320–321, 1992.